ERASMUS MUNDUS JOINT MASTER

SURFACE, ELECTRO-, RADIATION, AND PHOTO-CHEMISTRY

MASTER THESIS

STUDY OF THE QUANTUM EFFICIENCY OF THE EXCITONIC OPTICAL AMPLIFICATION OF NANOSENSORS BY LINEAR AND RAINBOW NONLINEAR OPTICAL SPECTROSCOPY

By

PHAM BA LICH

RESEARCH SUPERVISOR:

Christophe HUMBERT

ACKNOWLEDGEMENTS

I do thank to all people who helped me and supported me during the completion of this report.

Foremost, I especially would love to express my hearty appreciation toward Dr. Christophe Humbert for his continuous supervision, conscientious guidance, wonderful inspiration, and providing me with an excellent atmosphere during my thesis.

I would also like to acknowledge Assoc. Prof. Laurent Dreesen, and Dr. Thomas Noblet at University of Liege, Institute of Physics for their kind supports during my internship in Liege, Belgium. I also want to express a deep gratitude to Prof. Marie Erard, Institute of Physical Chemistry (ICP), University of Paris-Saclay and Prof. Bernard Humbert from Institut des Matériaux de Nantes (IMN) for helping me perform measurments on Time-resolved Fluorescence spectrocopy and Raman spectroscopy, respectively. I am gratefully indebted to them for their very valuable comments on this research topic.

My sincere thanks also go to Ms. Apolline Piard and Mr. Simon Jollet for their helpful support when practicing experiments in the laboratory. I also want to thank other lab mates and lab secretaries for all their kind supports.

Last but not least, I am grateful to staff of SERP+ program, four prestigious partner universities, Centre national de la recherche scientifique (CNRS) and the European Union for their support with kindness.

TABLE OF CONTENTS

List of abbreviations

APTES	(3-aminopropyl)triethoxysilane
EDX	Energy dispersive X-ray spectroscopy
HR-TEM	High-resolution transmission electron microscopy
IR	Infrared
NC	Nanocrystal
QD	Quantum dot
QD520	Quantum dot with fluorescence emission peak at 520 nm
QD570	Quantum dot with fluorescence emission peak at 570 nm
QD610	Quantum dot with fluorescence emission peak at 610 nm
SFG	Sum-frequency generation
XPS	X-ray photolelectron spectroscopy

Physical constants

$m_o = 9.1 \times 10^{-31}$ kg	Mass of electron
$R_H = 13.6$ eV	Rydberg's constant for the hydrogen atom
$\varepsilon_o = 8.85 \times 10^{-12}$ F/m	Dielectric permittivity of vacuum
$c = 3.0 \times 10^{8}$ m/s	Speed of light in vacuum
$k_B = 1.38 \times 10^{-23}$ J/K	Boltzmann's constant

ABSTRACTS

Quantum dots (zero-dimensional materials) are regarded as novel generation fluorescent probes confined in the size range of 1 to 10nm. In the field of bioimaging, the sensitivity of nanosensor is of pivotal importance to target the biomolecules, so this study focuses on the grafting of organic ligand-coated CdTe QDs monolayer with amine-terminated aliphatic organosilane APTES monolayer on glass surface to address the environmental problem and cost of nanosensors. QD monolayers samples were pre-characterized by UV-VIS absorption and fluorescence emission spectroscopies to benefit from the optical properties of QD on samples. Then Raman spectroscopy and non-linear SFG spectroscopy are two spectroscopic techniques for analyzing sample's chemical properties. The spectra modeling from UV-VIS, Fluorescence, and SFG were performed by Igor Pro software. The results of absorption and emission studies attest that the success of transferring the optoelectronic properties of QD from colloidal solution to APTES-modified glass samples. While QDs on glass exhibit a maximum absorbance at 477nm for QD520, 534nm for QD570, and 562nm for QD610, the emission peaks are detected at 512nm, 576nm, and 606nm, respectively. From time-resolved fluorescence spectroscopy, the effect of chemical structure of monolayers are seen from the fast-quenching phenomenon in relation to colloidal QDs solution. The analysis of Raman spectroscopy evidences the trace of chemical bonds from both APTES grafting molecules and QD's chemical ligands themselves. The consistency between Raman and SFG results is acknowledged by the presence of methylene and methyl groups in SFG spectra which come from both contributions of the organic layer of APTES and the molecular ligands of QDs. These analyses emphasize the dipolar coupling between QD's excitons and their molecular surroundings which improves the nanosensor's detection threshold.

Les points quantiques (matériaux de dimension zéro) sont considérés comme des sondes fluorescentes de nouvelle génération confinées dans la gamme de taille de 1 à 10 nm. Dans le domaine de la bioimagerie, la sensibilité du nanocapteur est d'une importance cruciale pour cibler les biomolécules. Cette étude se concentre donc sur le greffage d'une monocouche de QD CdTe couverts de ligands organiques sur une monocouche d'organosilane aliphatique APTES à terminaison amine, elle-même greffée sur une surface de verre pour résoudre le problème environnemental et le coût des nanocapteurs. Les échantillons de monocouches de QD ont été pré-caractérisés par des spectroscopies d'absorption UV-VIS et d'émission de fluorescence pour bénéficier des propriétés optiques des QD sur les échantillons. Ensuite, nous avons utilisé la spectroscopie Raman et la spectroscopie SFG non linéaire pour analyser les propriétés chimiques de l'échantillon. La modélisation des spectres UV-VIS, de fluorescence et SFG a été réalisée avec le logiciel Igor Pro. Les résultats des études d'absorption et d'émission attestent le succès du transfert des propriétés optoélectroniques des QD de la phase colloïdale à la phase solide sur substrat de verre silanisé par APTES. Alors que les QD sur verre présentent un maximum d'absorption à 477 nm pour QD520, 534 nm pour QD570 et 562 nm pour QD610, les pics d'émission sont localisés à 512 nm, 576 nm et 606 nm, respectivement. D'après la spectroscopie de fluorescence résolue en temps, l'effet de la structure chimique des monocouches se distingue de la solution colloïdale par une extinction rapide de la fluorescence. L'analyse de la spectroscopie Raman met en évidence la trace de liaisons chimiques provenant à la fois des molécules de greffage APTES et des ligands moléculaires des QD eux-mêmes. La cohérence entre les résultats Raman et SFG est attestée par la présence de groupes méthylène et méthyle dans les spectres SFG qui peuvent être considérés comme une contribution des ligands des QDs et de l'APTES. Ces analyses mettent l'accent sur le couplage dipolaire entre les excitons des QD et leur environnement moléculaire qui améliore la limite de détection du nanocapteur.

1. INTRODUCTION

For almost thirty years now, quantum dots (QDs), so-called “artificial atoms” have attracted a great attention in research due to their unique features. Quantum dots are classified as one type of inorganic nanoparticles including silver nanoparticles (AgNPs), gold nanoparticles (AuNPs), metal-organic frameworks (MOFs) [1]. Amongst these metal-based nanoparticles, quantum dots are semiconductor nanocrytals (1-10 nm) with valuable optical properties for nanosciences. They are the keystone of various applications and fields such as solar cells, transistors, laser diodes, photodectectors, biosensors, and molecular recognition devices for medical diagnosis [2-4]. One of the most fascinating properties of quantum dots is the tunable band gap due to the strong quantum confinement effect. Therefore, the optoelectronic properties (absorption and emission) of quantum dots may provide essential advantages in the visible spectral range to amplify the nonlinear optical (vibrational and electronic) response of the molecules around them.

Current research efforts are mostly directed at the biomedical imaging and detection applications (diagnostics, single molecule probes, and real-time imaging of tumors) of QD-based nanosensors [1, 4, 5]. In comparison with common organic dyes used as fluorescent emitters, semiconducting nanoparticles (quantum dots) possess distinct advantages of high resistance to photobleaching, good photo-stability, high brightness, high quantum yield [5-7]. With a broad absorption band and narrow emission spectra, quantum dots offer a flexible optical range of fluoresence which modulates the spectral overlap and enables to facilitate the biosensor sensitivity and improve dectection efficiency. Besides, quantum dots are also considered as one of the best donor candidates in Förster Resonant Energy Transfer (FRET)-based optical biosensors nowadays [8, 9]. Due to the ability for chemical conjugation with functionalizers (organic ligands) to activate the surface for biomolecule’s binding, quantum dots are promising fluorescent probes to detect targeting molecules.

In spite of the amazing optoelectronic properties and bio-application possibilities of QDs, an issue with the booming of electrical waste disposal is a critical problem for scientists and environmentalists. The manufacture of a great variety of biosensors is one of typical examples of this. By using metal-based nanosensors, the environmentally toxicity from core QDs can be potentially challenging during disposal, especially cadmium Cd if sensor products are manufactured by the conventional methods [4, 7]. In order to address this issue, the introduction of grafting by QD monolayer in nanosensors is necessary to both reduce the quantity of semiconductor QDs and synthesis-related chemicals for sensor production for green purposes and decrease the cost for material consumption. While quantitatively decreasing the waste of QDs material, the nanosensor performance is reliably as sensitive as conventional sensors.

In this internship, the quantum efficiency of the excitonic optical amplification of nanosensors was investigated in monolayers of commerical CdTe quantum dots deposited on another monolayer of anchoring agents (APTES) on glass substrate. The objectives here were to (1) implement and optimize the preparation of nanostructured samples in monolayers according to chemical protocols established at the ICP. (2) Secondly, the pre-characterization steps of quantum dots on glass were studied by UV-Visible spectroscopy and Fluorescence spectroscopy within the framework of an international long-term partnership funded by CNRS with University of Liège (Belgium). (3) Lastly, after achieving the optical responses of specific semiconductor nanocrystals targeted on glass, the evidence of molecular recognition system fabricated on glass will be exploited by Raman spectroscopy and by SFG spectroscopy in order to enhance the intensity of the molecular optical response at the surface of these nano-objects.

1.1. Quantum confinement effect and quantum dots (QDs)

Considering the number of degrees of freedom of movement (dimensionality of electrons), quantum nanostructures could be categorized into different classes. The number of degrees of freedom decreases so that the electrons are confined in more dimensions. Regarding the dimensionality of quantum structures, there are quantum wells (thin films), quantum wires, and quantum dots (QDs) (Figure 1) [10, 11].

Quantum wells (Q-wells) are present in fine semiconductor layers or thin film structures with a few nanometers in thickness and generally deposited on rigid substrates. The electron in Q-well is confined in one direction and there is no restriction of its movement in the two other directions. Thus, Q-wells are defined as two-dimensional (2D) materials.

Quantum wires (Q-wires) are nanowires or nanotubes in nanometer range of diameter and their lengths are of several micrometers. They are in needle-like structures. The electron in Q-wire is free to move in one dimension, then the remaining directions are quantized. Therefore, Q-wires are considered as one-dimensional (1D) structures.

Quantum dots (Q-dots or QDs) are nanocrystals or colloidal semiconductor nanocrystals (SNC). Electrons are restricted and quantized in all three directions. The concept of motion does not exist anymore for such electrons (in any direction), so QDs are classified into zero-dimensional (0D) materials.

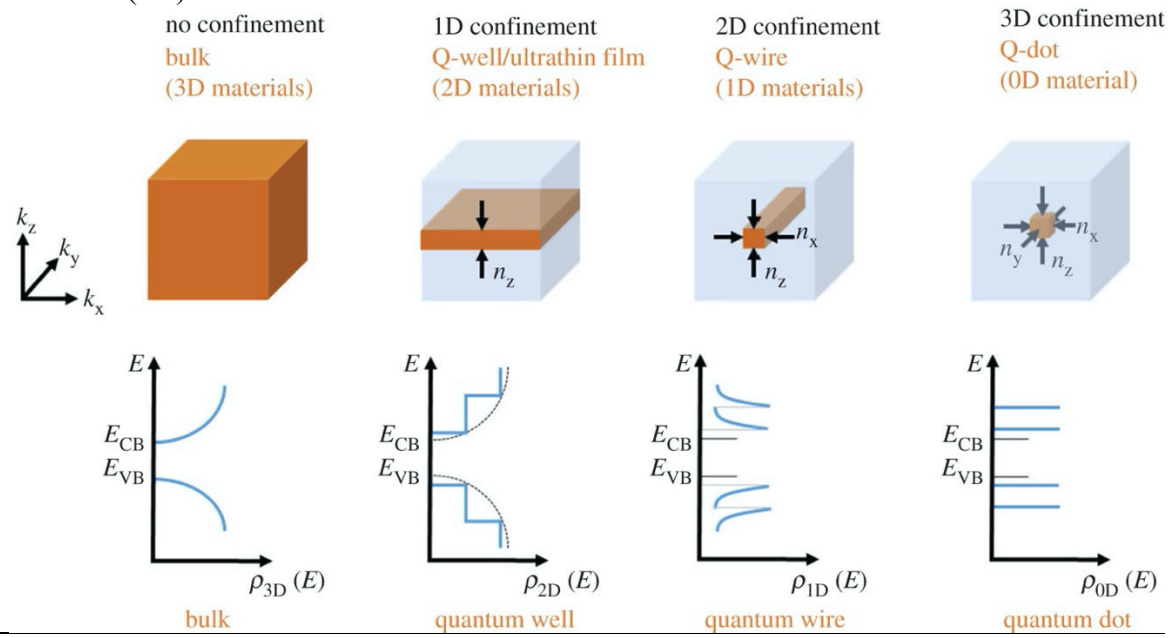

Dimensionality	3	2	1	0
Degree of confinement	0	1	2	3

Figure 1. Schematic demonstration of low-dimensional quantum confinement systems and their energy levels via density of sates (DOS) of electron. This image was reprinted from reference [12] ($\rho(E)$: density of state of electron, E_{CB}, E_{VB} are energy levels of electron in conduction band and valence band, respectively)

To understand the quantum confinement effect of electron, it is crucial to know the formation of quasiparticle – exciton (Figure 2) [13]. In semiconductors, the energy separation between valance band and conduction band is called band gap E_g which is a finite and specific value for each different semiconductor material. As an electron (-e) was excited with sufficient energy from thermal excitation or photon absorption (hv), it will escape from valence band and jump over the energy gap to reach the conduction band. Therefore, a so-called quasiparticle "hole" is left behind in valence band with opposite charge (+e). A hole is an electron vacancy in the valence band. This phenomenon creates the charge carriers in semiconductors or the recombination of electron-hole pair after a finite time with the release of energy. However, in quantum dots, when the size or radius of crystals approaches to "Bohr radius", the excited electron (e-) and its hole (h+) experience the electrostatic Coulomb interaction (attraction

force) and form a bound electron-hole pair named as "exciton". Electrically, exciton is a neutral quasiparticle with an average physical separation between electron and hole. This distance is referred as exciton Bohr radius a_B and ranges from 1 to 10 nm for quantum dots. Each semiconductor materials is characterized by a specific value of the exciton Bohr radius [11].

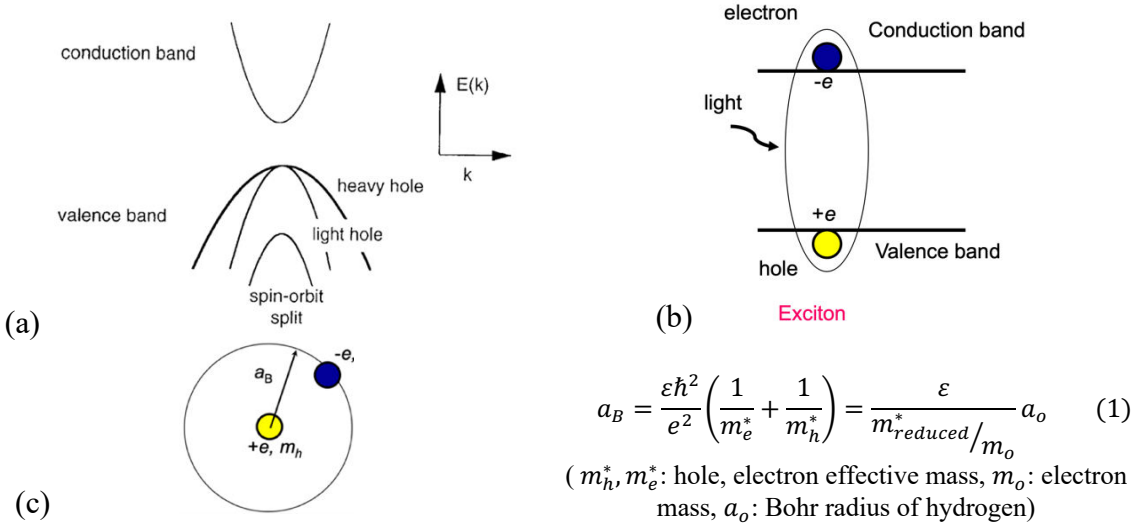

$$a_B = \frac{\varepsilon\hbar^2}{e^2}\left(\frac{1}{m_e^*}+\frac{1}{m_h^*}\right) = \frac{\varepsilon}{m^*_{reduced}/m_o} a_o \qquad (1)$$

(m_h^*, m_e^*: hole, electron effective mass, m_o: electron mass, a_o: Bohr radius of hydrogen)

Figure 2. Schematic diagram showing the formation of excitons in QD energy band (2a and 2b), and exciton Bohr radius (2c). Figure 2a was reprinted from Ref. [14]. Equation (1) is the formula for exicton Bohr radius [1].

Whilst non-confined motion of charge carrier including electron or exciton (electron-hole quasiparticle) and original-kept band gap are seen in bulk nanomaterials, QDs are nanosize crystals with size-dependent band gap [15]. Moving from bulk materials to quantum dots, it is clear that the continuous electronic bands are split up into discrete energy levels and the higher surface-to-volume ratio (many atoms at the surface of the crystallite lattice) is more evident (Figure 3). The changes of band gap of semiconductor crystals lead to their dramatic variation of optical properties such as absorption and emission [13]. These changes can be ascribed to quantum confinement effect. The concept of quantum confinement can be dissected by breaking the words into "quantum" and "confinement". Quantum represents the atomic realm of particles and the quantization of a particle gives the discrete specific energy levels. Confinement is related to the restriction of particle's motion. The quantum confinement effect can vary several properties of semiconductor QDs, including magnetic properties and conductivity [14]. Amongst them, the size- and shape-dependent optoelectronic properties (absorption spectrum and emission colour) are the most interesting phenomena deriving from quantum confinement.

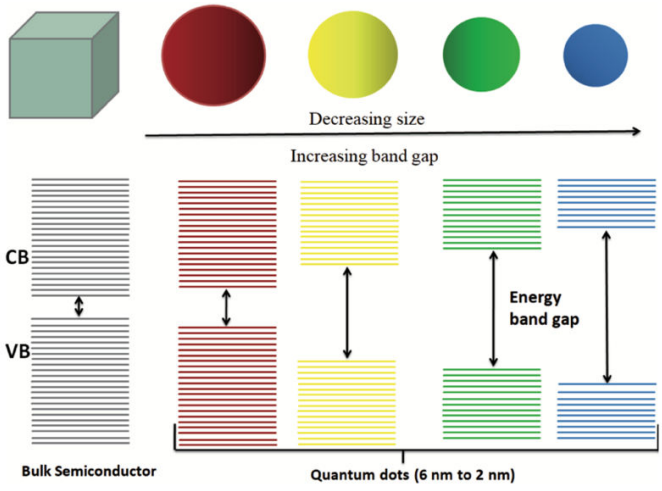

Figure 3. Schematic illustration of the dependence of energy band on the size of QDs. This image was reprinted from Ref. [16]

The quantum confinement effect will appear as the reduction in semiconductor nanocrystal's size reaches to nano scale in comparison to the critical quantum limit which is the charge carrier Bohr radius ($r \leq a_B$). Then, the motion of electrons and holes is spatially confined to the dimension of the QD. In this circumstance, the decrease in dimensionality produced by confining electrons (and holes) generates the discrete energy states with k_BT energy difference (k_B: Boltzmann constant) and widens up the band gap between the highest valence band (HOMO) and the lowest conduction band (LUMO). Therefore, the size-dependent absorption and emission of QDs with discreteness of electron spectra predominantly depends on the nanocrystal's size distribution ($r \leq 10$ nm) [14].

One of the most important consequences of the increase of quantum confinement effect in quantum dots is an increase in energy of the band-to-band excitation peaks (E_g) leading to the decrease of emission wavelength. Hence, the blue shift in the emitted light occurs as the particle's size is decreased (Figure 4). In fluorescent dye applications, the frequency of emitted light increases as the size of the quantum dot decreases, shifting the color of emitted light from red to violet [14].

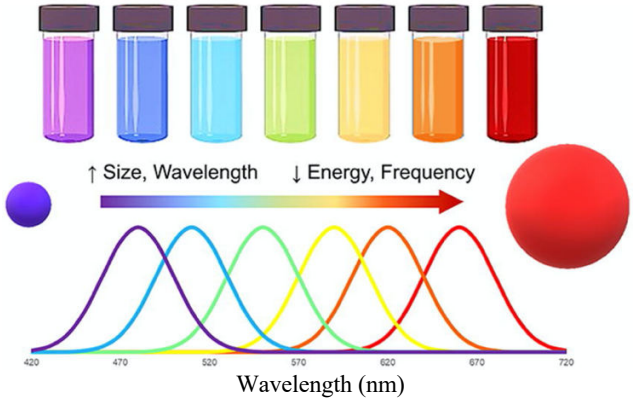

Figure 4. Schematic picture of the variation of optical properties of QDs as the size is changed. This image was reprinted from Ref. [17]

1.2. CdTe QDs' structure and optical properties

The classification of quantum dots is based on the composition and structure of their materials. In general, there are three different types of QDs including core-type QDs, core-shell QDs, and alloyed QDs [18, 19]. To be particular, core-type QDs are nano dots made from single-element component (Si or Ge) or from compound semiconductors with uniform internal compositions such as chalcogenides with metals (CdSe, PbSe, CdTe, and PbS…). This type of QDs is applicable for the study of photo- and electroluminescence properties due to their tunable band gap and emission color. Secondly, core-shell QDs are QDs which are coated with shells of another higher band gap semiconducting material to enhance quantum yield. Take CdSe QDs as an example: CdSe is in the core while ZnS is in the shell surrounding CdSe. The method of coating the shell around the core has been widely developed to investigate the photophysical properties of QDs. Lastly, in the case of size restrictions, alloyed QDs such as CdS_xSe_{1-x}/ZnS (x is composition variable) are the alternative approach to tune the optical and electronic properties by varying the internal element's composition in QDs. Different types of QDs with the ranges of emission wavelengths are indicated in Figure 5.

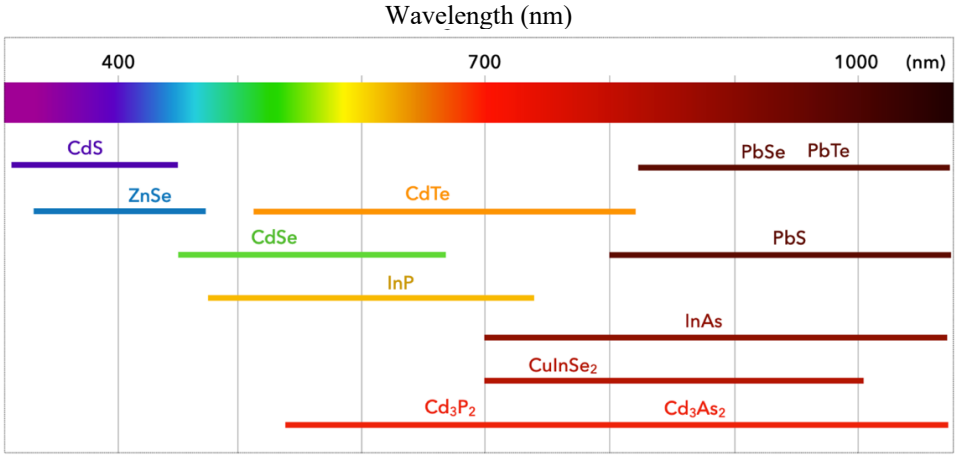

Figure 5. Optical activity of semiconductor quantum dots. This figure was reprinted from Ref. [20]

Amongst several kinds of QDs, CdTe QDs possess a small band gap (around 1.6 eV for QD775) so that their band gap can be tuned to absorb light and emit fluorescence in the visible spectral range. When the size of CdTe QDs is in diameter of less than 10 nm, the quantum confinement effect is strong. Furthermore, the surface of CdTe QDs can be easily modified with other functional groups, especially hydrophilic groups to make them dissolve in water and obtain colloidal solutions. CdTe QD will be used in the internship.

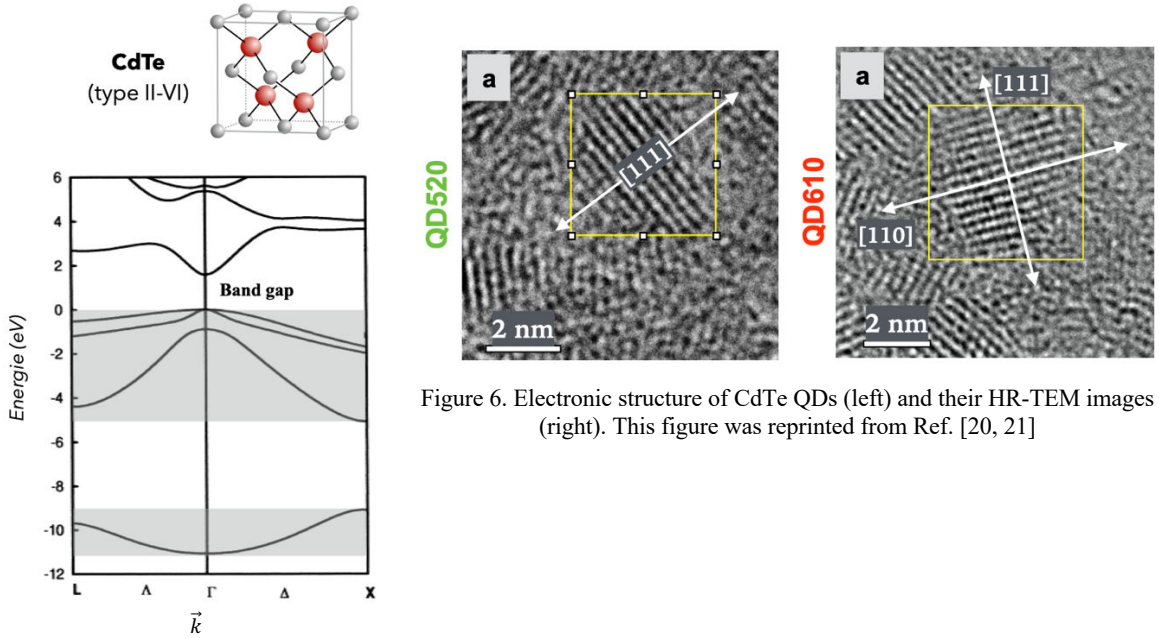

Figure 6. Electronic structure of CdTe QDs (left) and their HR-TEM images (right). This figure was reprinted from Ref. [20, 21]

Regarding the structural properties of CdTe QDs, based on previous studies [20-22] on commerical CdTe QDs functionalized with COOH groups, they belong to type II-VI alloy QDs which is not core-type QD as stated by the manufacturer and the crystal structure of CdTe QDs is cubic zinc-blende (ZnS) structure. From high-resolution transmission electron microscopy (HR-TEM) analysis [20, 21], CdTe QDs are in the shape of facets which are not coincident with the assumption of simple spherical model of QDs (Figure 6). The mean diameters of different QDs were also investigated and showned in the next section of CdTe QDs preparation.

In terms of chemical characterization, it was concluded from energy dispersive X-ray spectroscopy (EDX) and X-ray photolelectron spectroscopy (XPS) measurements that CdTe QDs have a 75% S/Te ratio and consist of ternary alloy $CdTe_xS_{1-x}$ (x = 0.25). It was revealed that the molecular ligand conjugated with QDs is mercaptopropionic acid HS-$(CH_2)_n$-COOH (n = 2) [23].

For $CdTe_{0.25}S_{0.75}$ QDs, the excitonic states were written as the tensor product of electron's state function and hole's state function following the formula below:

$$|v>_X = |n\ell>_e \otimes |n'\ell'>_h$$

And the eigenenergy of the v^{th} excitonic state was given by the following equation [11, 20]:

$$\hbar\omega_v = E_g + \frac{\kappa_v}{R^2} - \frac{\eta_v}{R} \qquad (2)$$

where $\kappa_v = \kappa_{n\ell,n'\ell'} = \frac{(\hbar\alpha_{n\ell})^2}{2m_e} + \frac{(\hbar\alpha_{n'\ell'})^2}{2m_h}$ (eV.nm^2) and $\eta_v = \eta_{\ell,\ell'} = \frac{c_{\ell,\ell'}e^2}{4\pi\varepsilon_o\epsilon_r}$; $\frac{\kappa_v}{R^2}$ are the confinement energies of the electron (e) and the hole (h) whilst $\frac{\eta_v}{R}$ is the Coulomb attraction potential of electron-hole pair. R is the radius of QDs, E_g is band gap energy of bulk CdTe (E_g=1.61 eV at 4K), and ϵ_r is the dielectric constant of bulk CdTe (ϵ_r = 10.3).

As given in Figure 7, the values of coefficients κ_v and $c_{\ell,\ell'}$ of the first six excitonic states of $CdTe_{0.25}S_{0.75}$ QDs are indicated. κ_v coefficients were calculated and determined from the experimental characterizations. These are spectroscopic characterizatic coefficients of UV-VIS absorption and fluorescence emission, which allow deducing the values of the effective masses of electron, heavy hole and light hole (m_e= 0.17m_o ; m_{hh}= 1.96m_o ; m_{lh} = 0.44m_o).

(a)

$\lvert\nu\rangle_X$	$\lvert n\ell\rangle_e \lvert n'\ell'\rangle_h$	$\kappa_{n\ell,n'\ell'}$	$c_{\ell,\ell'}$
1	$1s_e\ 1s_{hh}$	2,39	1,78
2	$1s_e\ 1d_{hh}$	2,84	1,52
3	$1s_e\ 2s_{hh}$	2,96	1,78
4	$1s_e\ 1s_{lh}$	3,05	1,78
5	$1s_e\ 2d_{hh}$	3,80	1,52
6	$1p_e\ 1p_{hh}$	4,89	1,53

(b)

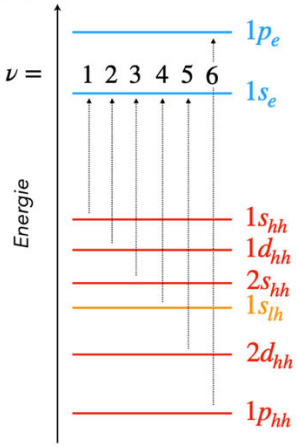

Figure 7. Excitonic states of $CdTe_{0.25}S_{0.75}$ QDs. This figure was reprinted from Ref. [20]

In this report, the modelisation of UV-VIS absorption and fluorescence emission spectroscopies will be studied to establish a systematic understanding about optical properties of different QDs in colloidal solution and on glass substrate by adopting Igor software. During the fitting, the experimental data is presented in circle marker mode while the fitting is indicated in thin line.

1.3. Principles of UV-VIS spectroscopy

Due to the nature of discrete states in the quantum systems, the optical susceptibility of CdTe quantum dots is expressed as [11, 20]:

$$\chi^{(1)}_{QD}(\omega) = -\frac{N}{\hbar\varepsilon_o}\sum_{v\neq 0}|p_v|^2\left(\frac{1}{\omega-\omega_v+i\gamma_v} - \frac{1}{\omega+\omega_v+i\gamma_v}\right) \qquad (3)$$

where N is the QD density, v is the label/index of excitonic states, p_v is the dipole moment in the v^{th} exciton, and γ_v , ω_v are the damping constant and the eigenenergy, respectively. ω_v is calculated by equation (2). The values of p_v are experimentally determined.

The UV-VIS absorbance of a colloidal solution of QDs is directly proportional to the effective absorption section $\sigma_a(\lambda)$ (m^2) of QDs and the optical pathway or the length of cuvette ℓ (m) (ℓ =0.01m).

$$A(\lambda) = \frac{N\ell\sigma_a(\lambda)}{ln10}$$

As the absorption cross section of QDs $\sigma_a(\lambda)$ only depends on the imaginary part of $\chi_{QD}^{(1)}$, the absorbance A_R is described as

$$A_R(\omega) = \frac{\ell}{c\ ln10} \times \frac{\omega}{\sqrt{\epsilon_r}} \times \frac{N}{\hbar\varepsilon_o} \times \sum_{v\neq 0} |p_v|^2 \frac{{\gamma_v}^2}{(\omega-\omega_v)^2 + {\gamma_v}^2} \qquad (4)$$

Furthermore, the size of QDs (radius R) affects on the frequencies of QDs (ω_v). Hence, the absorbance with a Gaussian distribution of the radius is considered to the size dispersion of QDs. R_o is the mean radius and $\sigma(R)$ is the standard deviation.

$$A(\omega) = \int_0^{+\infty} dR\ A_R(\omega) \frac{\exp\left(-\frac{(R_v(\omega)-R_o)^2}{2\sigma(R)^2}\right)}{\sigma(R)\sqrt{2\pi}} \qquad (5)$$

Mathematically, by applying Lorentzians approximation, it reduces to

$$A(\omega) = \frac{N\times\ell}{c\ ln10} \frac{\omega}{\hbar\varepsilon_o} \frac{1}{\sigma(R)} \sqrt{\frac{\pi}{2\epsilon_r}} \sum_{v=1}^{6} \frac{|p_v|^2}{G_v(\omega)} \exp\left(-\frac{(R_v(\omega)-R_o)^2}{2\sigma(R)^2}\right) \qquad (6)$$

This equation (6) is applied for absorption of a colloidal solution of QDs with known concentration. For QDs deposited on glass samples, the absorbance will depend on the surface density of QDs. Therefore, the product of $N\times\ell$ will be replaced by N_s in the equation.

$$A(\omega) = \frac{N_s}{c\ ln10} \frac{\omega}{\hbar\varepsilon_o} \frac{1}{\sigma(R)} \sqrt{\frac{\pi}{2\epsilon_r}} \sum_{v=1}^{6} \frac{|p_v|^2}{G_v(\omega)} \exp\left(-\frac{(R_v(\omega)-R_o)^2}{2\sigma(R)^2}\right) \qquad (7)$$

where

$$R_v(\omega) = \frac{-\eta_v + \sqrt{{\eta_v}^2 + 4(\hbar\omega - E_g)\kappa_v}}{2(\hbar\omega - E_g)} \quad \text{and} \quad G_v(\omega) = \frac{2\kappa_v}{\hbar R_v^3(\omega)} - \frac{\eta_v}{\hbar R_v^2(\omega)}$$

In the fitting procedure on glass samples, the only two fitting parameters are the surface density N_s and the size dispersion $\sigma(R)$ due to these other known parameters in colloidal QD solutions from previous determination. Examples of application of such procedure are given in section 3.1.1.

1.4. Principles of fluorescence emission

The nature of classical optical process of fluorescence leads to the Lorentzian spectrum in the fluorescence emission [9].

$$I_f(\omega) \ \propto\ \frac{1}{\pi} \frac{\gamma_f}{\left(\omega-\omega_f\right)^2 + {\gamma_f}^2} \qquad (8)$$

By applying the similar approach as UV-VIS absorption spectrum, the Gaussian distribution of the radius R was adopted for fluoresence intensity and the emission energy of the first excitionic state ($v = 1$) is lowered by a quantity $\Delta_{St.}$ corresponding to the Stokes shift. Stokes shift is the displacement (energy difference) between the absorption and emission maxima due to the non-radiative processes such as vibrational relaxation and internal conversion revealed by the Jablonski diagram.

$$\hbar\omega_f(R) = E_g - \Delta_{St.} + \frac{\kappa_1}{R^2} - \frac{\eta_1}{R} \qquad (9)$$

Then, we have:

$$I_f(\omega) = \frac{F_o}{\sigma\sqrt{2\pi}} \frac{\exp\left(-\frac{(R_f(\omega)-R_o)^2}{2\sigma(R)^2}\right)}{G_f(\omega)} \qquad (10)$$

where

$$R_f(\omega) = \frac{-\eta_1 + \sqrt{{\eta_1}^2 + 4(\hbar\omega - E_g + \Delta_{St.})\kappa_1}}{2(\hbar\omega - E_g + \Delta_{St.})} \quad \text{and} \quad G_f(\omega) = \frac{2\kappa_1}{\hbar R_f^3(\omega)} - \frac{\eta_1}{\hbar R_f^2(\omega)}$$

In the fitting procedure, the amplitude F_o, the Stokes shift $\Delta_{St.}$, and the standard deviation $\sigma(R)$ are the fitting parameters. Illustrations of application of such procedure are indicated in section 3.1.2.

1.5. Principles of Time-Resolved Fluorescence Spectroscopy

To understand the change in fluorescence time of QDs, Time-Resolved Fluorescence spectroscopy is the efficient method to characterise their emission. The fluorescence emission intensity is proved that it is followed by sum of multi-exponential function with different lifetimes τ_n.

$$I_f(t) = \text{Background} + \sum_{n=1}^{c} A_n e^{\frac{-t}{\tau_n}} \qquad (11)$$

where $I_f(t)$ is fluorescence intensity depending on time t, A_n is the amplitude of fluorescence corresponding to each lifetime τ_n.

The fluorescence decays of colloidal QDs were studied by acquiring the fluorescence decay times τ_n from the triple exponential function ($c = 3$). In QD monolayers, the fluorescence decays are assumed to be a sum of four exponentials ($c = 4$). The determination of the number of exponentials applying for colloidal QDs and QD monolayers is simply from mathematical meaning in order to obtain the best fitting line and up to four exponentials are sufficient to explain the data.

The average lifetime is evaluated by the following equation (12) and the fitting examples are shown in section 3.1.3.

$$\tau_{n_{ave}} = \frac{\sum_{n=1}^{c} A_n \tau_n}{\sum_{n=1}^{c} A_n} \qquad (12)$$

1.6. Spectroscopic methods for chemical characterization of QD monolayers on glass substrate

Despite the evidence of QDs assembly on glass from UV-VIS absorption and fluorescence pre-characterization, the chemical understanding about surface structure of QD monolayers on glass should be taken into consideration to fortify the hypothesis of QD monolayers. Amongst analytical techniques to study the chemical structure, Raman spectroscopy is suitable because it is a non-destructive optical probe for the sample. Another advanced technique to see the interaction between QDs and APTES monolayers is the sum-frequency generation spectroscopy (SFG).

1.6.1. Raman Spectroscopy

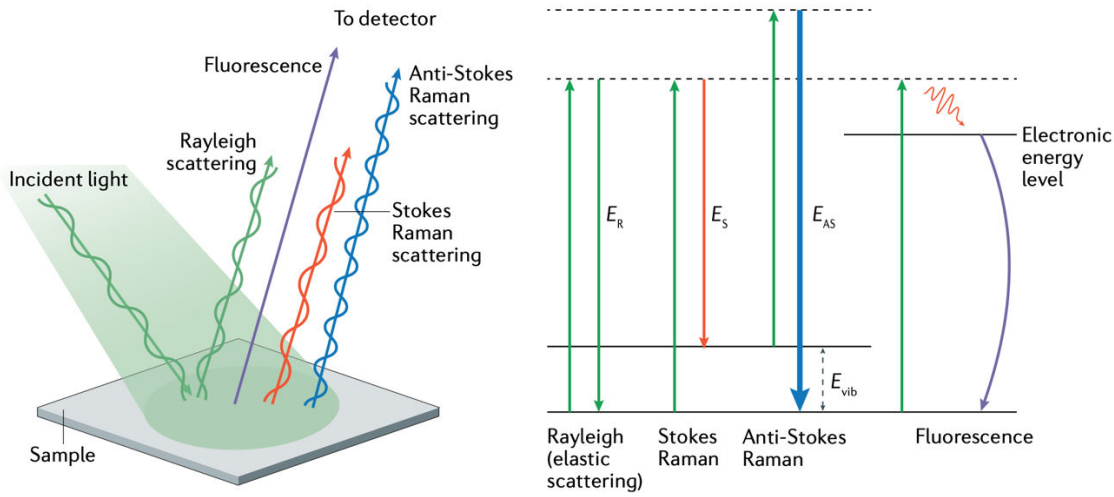

Figure 8. Fluorescence and Raman scattering. This image is reprinted from [24].

Raman spectroscopy is both qualitative and quantitative analytical technique which provides details about chemical structure, phase, crystallinity, and molecular interactions. The principle of Raman technique is based on the interaction of incident light generated from a high intensity laser with the chemical surface structure of material (Figure 8). On the one hand, the wavelength of the main part of the scattered light is unchanged with respect to the laser source and thus does not bring useful information. This light scattering is called Rayleigh scattering. On the other hand, the phenomenon for which a small amount of light (around 10^{-7} %) scatters with different wavelength compared to incident light is named as Raman scattering. Raman shift (wavenumber cm^{-1}) is defined as the difference between the frequencies of incident and scattered light. If the Raman shift with $\lambda_{scattered} > \lambda_{incident}$, this is the Stokes Raman scattering. Otherwise, it is referred as Anti-Stokes Raman scattering when $\lambda_{scattered} < \lambda_{incident}$. A Raman spectrum profile illustrates peak's positions and their relative intensities of the chemical structure of analytes. Each peak matches with vibration of a specific chemical bond and functional group. Hence, the spectrum presents a distinct chemical fingerprint which helps to qualitatively identify a particular molecule or material and distinguish from others as well as quantitatively determine the concentration of analytes based on peak intensities. The chemical identification can be resolved by using Raman spectral libraries to find a match with analyte's data.

1.6.2. Sum-Frequency Generation Spectroscopy

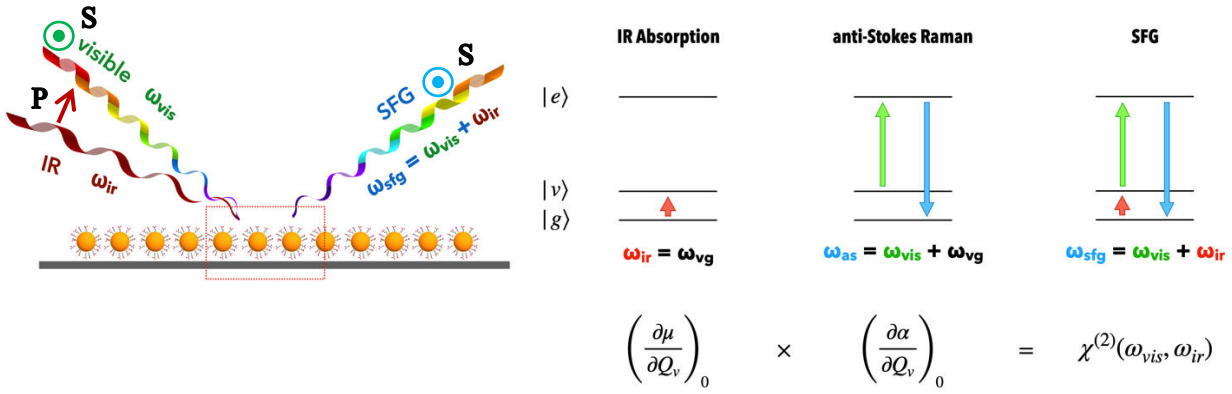

Figure 9. Sum-frequency generation at nanostructured interfaces (left) in SSP (SFG, Vis, IR) polarization configuration and vibrational spectroscopies (right). This figure is reprinted from [25].

From optical spectroscopic point of view, the polarization of materials $P(\omega)$ is defined as [25]:

$$P(\omega) = \varepsilon_o \chi^{(1)} E(\omega) + \varepsilon_o \chi^{(2)} E(\omega)^2 + \varepsilon_o \chi^{(3)} E(\omega)^3 + \cdots \qquad (13)$$

where $P(\omega)$ is molecular polarization, $E(\omega)$ is electric field, $\chi^{(n)}$ are electric susceptibility of n^{th} order. In linear optical processes (first order) such as refraction, absorption, diffusion, extinction, their polarization is the first term ($P(\omega) = \varepsilon_o \chi^{(1)} E(\omega)$). Nonetheless, the polarization of non-linear processes (normally second and third order) also contains latter terms. While Raman processes, fluorescence, optical Kerr effect are third order processes, sum-frequency generation spectroscopy (SFG) is a non-linear second order optical process (three-photon process). It allows to probe the vibrational and electronic properties of materials. Therefore, SFG is the simultaneous combination of two processes in a molecule: an infrared absorption and an anti-Stokes Raman process as depicted in Figure 9. Therefore, by energy conservation law, ω_{SFG} is calculated by: $\omega_{SFG} = \omega_{VIS} + \omega_{IR}$.

At the molecular level, an SFG process can be active if and only if the molecular hyperpolarisability is simultaneously Raman and Infrared active, which is almost the case for species adsorbed at interfaces. For centrosymetric materials, it can be shown that their nonlinear second order susceptibility $\chi^{(2)}$ is zero because of the centrosymmetric character of their electronic properties within the dipolar approximation. As a consequence, at the interface between two different centrosymmetric materials, we have a symmetry breaking of the electronic properties. Therefore, $\chi^{(2)}$ is always different from zero at any surface or interface and SFG is known as intrinsically surface sensitive spectroscopy.

2. MATERIALS AND METHODS

2.1. Chemical protocols

2.1.1. Preparation of CdTe QDs

CdTe (Cadmium Telluride – 240.01g/mol) QDs in water-soluble powder form were purchased from Sigma Aldrich manufacturer (Saint-Quentin-Fallavier, France). In this study, there are 3 different CdTe core-type QDs investigated: Ref. 777935 – 10 mg, Ref. 777943 – 10 mg, and Ref. 777951 – 25 mg which are named as QD520, QD570, and QD610, respectively. These notations are based on the fluorescence emission peaks in nm of each QD claimed by the manufacturer. These commercial QDs were functionalized with carboxylic acid groups (COOH) on the surface (Figure 10 and 11a). These ligands were determined to be mercaptocarboxylic acids HS-$(CH_2)_n$-COOH ($n \leq 3$) [23]. The stock solutions was prepared by adding MilliQ water (18MΩ.cm, Millipore, Orsay) and dissolving thoroughly with shaking. Hereafter is the details of concentrations and information of different QDs (Table 1).

Table 1: Specific details on different QDs stock solutions

QDs	Fluorescence at λ_{em} (nm)	Reference no.	Diameter (nm)	V (H_2O added) (mL)	Stock concentration $\times 10^5$ (M)	QD density (m^{-3})
QD520	520	777935	3.4 ± 0.6	2.6	3.92	2.36×10^{22}
QD570	570	777943	3.6 ± 0.5	2.6	3.30	1.99×10^{22}
QD610	610	777951	3.8 ± 0.7	2.8	6.52	3.93×10^{22}

QD520 QD570 QD610

Figure 10. Image showing the colors of QDs stock solutions

2.1.2. Chemical protocol for deposition of CdTe QD monolayers on glass

In this procedure, all the chemicals were from Sigma-Aldrich grades with 99.8% purity unless otherwise stated. Organic chemicals adopted during protocol are acetone Ace (99.8%), absolute ethanol EtOH (99.8%), anhydrous methanol MeOH (VWR-99.9%), and (3-aminopropyl)triethoxylsilane (APTES, A3648-100mL, ≥ 98%) solution (Figure 11b). Inorganic piranha solution was prepared from a mixture of concentrated hydrogen peroxide (H_2O_2 30% w/w) and concentrated sulfuric acid (H_2SO_4 VWR-95%) in the volume ratio of 1:2. Milli-Q millipore water with 18 MΩ.cm resistivity was used for all dilutions except APTES preparation. N_2 gas is from ALPHAGAZ 1, 200 bars, M20, 1066 compressed gas. The glass substrates were purchased from VWR (ref. 631-1551 Microscope slides, borosilicate glass).

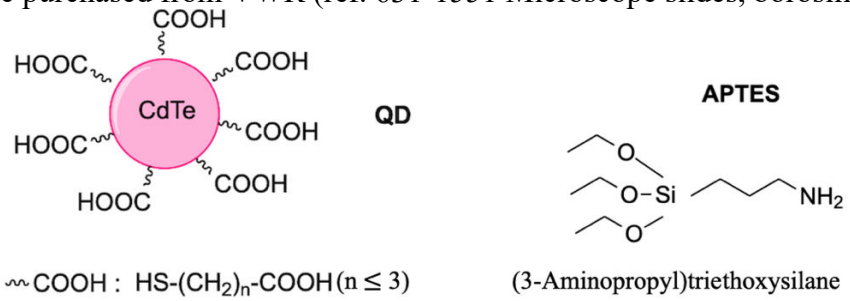

Figure 11. Chemical structure representation of QD (left) and APTES molecule (right)

The monolayers of QD and APTES on glass substrate were obtained by a wet chemistry protocol previously applied on gold nanoparticles [26, 27]. In general, there are three main

steps as follows Figure 12: (1) the cleaning process using different organic solvents to remove any impurity from the substrates and hydroxylation with piranha solution, (2) the deposition of an APTES monolayer acting as NH_3^+-positive head on the substrate to facilitate the next QD grafting layer serving as COO^--negative head, and (3) the deposition of a monolayer of QDs via electrostatic interaction (physisorption strategy) by dipping the silanized substrates in a colloidal QD solution. The reason why there are ionic bonds between QDs and APTES is that under aqueous medium of colloidal QDs solution (pH 5.5), the protonation of APTES molecules (pK_a(-NH_2) ≈ 10) has occured and the measured zeta potential ζ of COOH-coated CdTe is -36 mV which means that colloidal CdTe solution is stable and the surface charge is negative [22]. The schematic representation of chemical strategy of QD monolayers deposition on glass substrate is summarized in Figure 12 and QD monolayers is depicted in Figure 13.

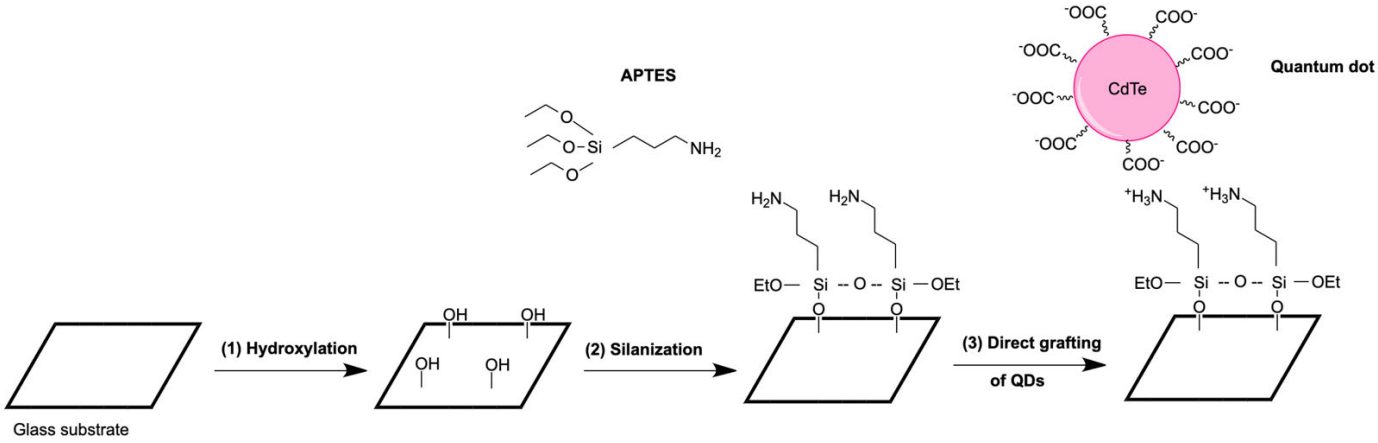

Figure 12. Chemical strategy of monolayers deposition of APTES and QDs on glass substrate. This figure was adapted from Ref. [22]

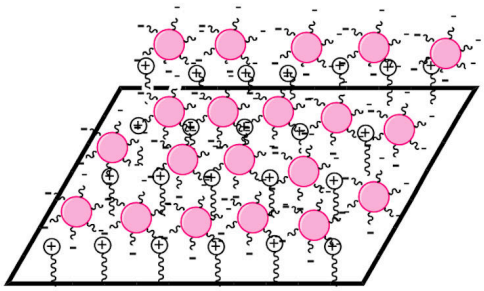

Figure 13. Schematic illustration of monolayer of APTES and QDs on glass substrate

To be more specific, (1) the cleaning step with organic solvents was performed under sonication by Fisherbrand FB15051 sonicator for five minutes per solvent. First, we start washing the substrate with CH_3COCH_3 to remove grease or any organic contaminants attached on the surface of substrate. The following alcohol cleaning step with EtOH was applied for discarding the Ace solvent. Then, the substrate was rinsed thoroughly in MilliQ water and dried under N_2 flow before immersing in a piranha solution. The immersing time for hydroxylation is 10 minutes. This step makes sure the total removal of the residual organic particles by hydrolysis and activates the surface of substrate by forming hydroxyl (-OH) groups. After that, another rinsing with excessive of MilliQ water and drying with N_2 gas were performed. (2) To silanize on hydroxylated samples, we used a 5% (w/v) solution of APTES prepared in anhydrous MeOH 99.9%. Equivalently, to achieve 5% APTES solution in 100mL of MeOH, it requires 5.0 g of APTES stock solution. For each substrate, 4 mL of 5% APTES solution is sufficient, and the immersion of APTES occurs in one and a half hour under a fume hood at 20 ^oC. Next, the silanized samples were sonicated (four times and one minute per time) in the step of rinsing with fresh MeOH to get rid of multilayer absorption. After APTES monolayered

substrates were dried under N_2 flow, they were proceeded into the deposition of QDs. (3) To graft QDs on the silanized samples through electrostatic interaction, it is optimally preferable to leave these samples immersed in 4 mL 0.5μM colloidal QD solution diluted from stock QD solution for two hours. Lastly, the QD-monolayered sample was rinsed with MilliQ water, and dried under N_2 flow. Eventually, all dried samples were stored in separate plastic boxes and covered by alluminium foil in a fume hood at 20 ^oC until their optical measurements. The chemical protocol was depicted in Figure 14.

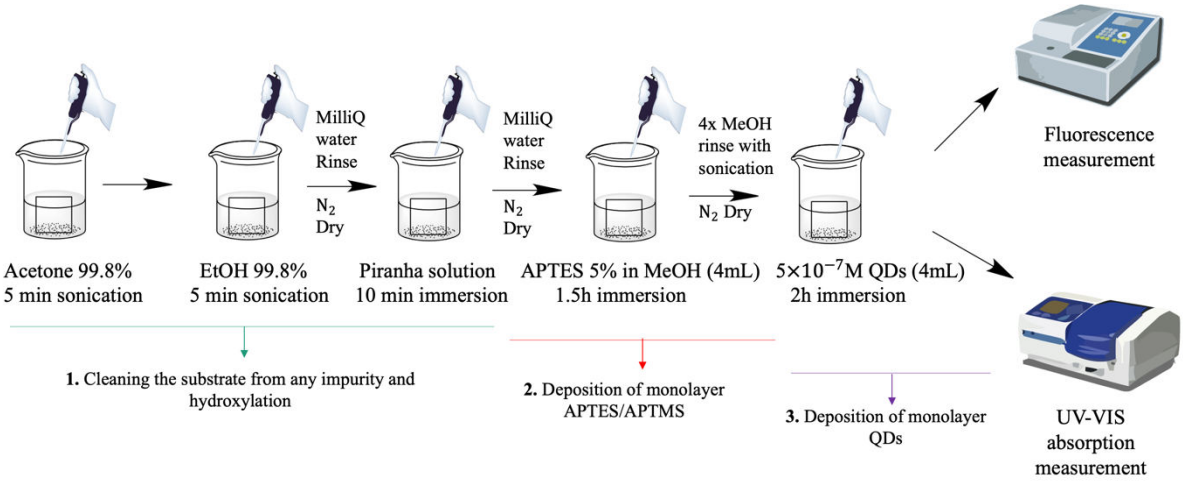

Figure 14. Schematic illustration of steps to deposit QDs on glass

2.2. UV-VIS absorption spectroscopy setup

To study the optical properties of QDs, UV-VIS absorbance spectroscopy of QDs was investigated. For both colloidal QD solutions and the QD-deposited samples, UV-VIS absorbance spectra were acquired by Cary Series UV-Vis-NIR Spectrophotometer 5000 (Agilent) in transmission (Figure 15). Regarding the reference samples, MilliQ water was used for reference signal in a PMMA cuvette (1 cm length) because it serves as a solvent in QD solutions while a bare glass substrate with the same thickness used in QD deposition on glass was measured for reference. The QD spectra in colloidal solution and glass substrate are both recorded from the difference of the absorbance of the sample and the reference.

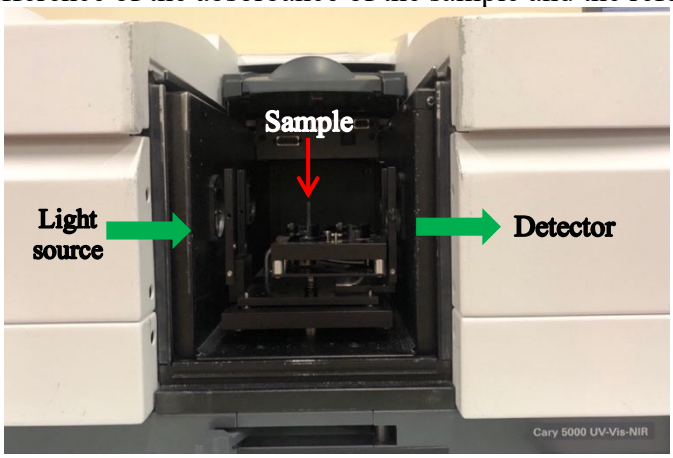

Figure 15. Schematic representation of UV-visible absorption measurement

2.3. Fluorescence spectroscopy setup

The fluorescence emission spectroscopy of QDs was also investigated to see the emission band of QD in solutions and glass substrates. The fluorescence spectra were recorded in Liège by using an Horiba IHR-320 spectrofluorometer coupled with an SR-830 lock-in amplifier (Stanford Research System). The emission wavelength of the UV lamp is 310 nm and the right angle geometry was the usual geometry for measuring the fluorescence. The

fluorescence performances were experimented in Belgium thanks to a long-term collaboration between University of Liège and French CNRS international counterpart funded for Innovative Nanostructure for Medical and Photocatalytic Application (INANOMEP) project. The configuration and experimental set-up scheme is depicted in Figure 16.

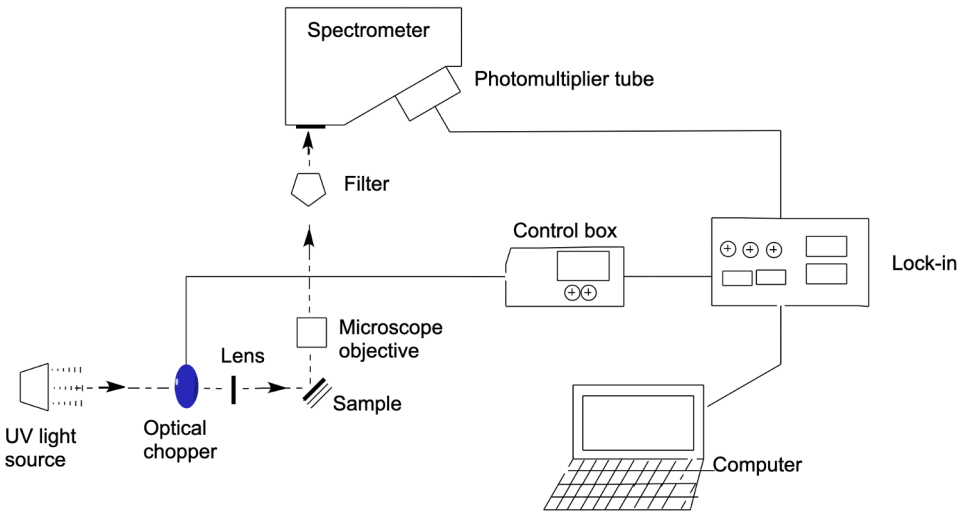

Figure 16. Schematic representation of fluorescence measurement

2.4. Time-resolved fluorescence spectroscopy setup

The study of fluorescence decays of QDs was investigated by using a custom-made time-resolved laser scanning time-correlated single photon counting microscope (TCSPC). To be more specific, a TE2000 microscope with a 60×/1.2 NA water immersion objective (Nikon) was set up with a 400 nm pulsed laser diode (LD) to acquire TCSPC path. A 520/28 nm bandpass filter was chosen to acquire the fluorescence before detecting by an MCP-PMT dectector (Hamamastu Photonics). The time for each pulse of excitation is 120 picoseconds and the time interval between two alternative pulse is 50μs. The data are recorded by the SymPhoTime 64 software (PicoQuant) and the decays were treated with fitting procedure of an exponential function (IgorPro software). This experiment was performed with the assistance of Prof. Marie Erard (ICP, University of Paris-Saclay).

2.5. Raman spectroscopy setup

The schematic configuration of Raman spectrometer is given in Figure 17. Raman spectra were recorded using a microconfocal Raman Invia Reflex device. The instrument was equipped with a double edge filter to eliminate the Rayleigh scattering, and a Charged Couple Device (CCD) camera working at a temperature of 220 K with a 1024 by 256 pixels array. Laser excitations were at 488nm, 514 nm, and 633nm. The setup was composed of a confocal microscope that was equipped with an automated XYZ table, where the piezo motors were able to generate 100 nm steps with a spatial precision better than 100 nm verified on an AFM grid. The spectral resolution achieved with the use of gratings of 2400, 1800 or 1200 grooves per millimetre was between 3 and 4 cm^{-1} according to the excitation wavelength. For each sample, twenty spectra were recorded at different areas of the sample to check for a potential heterogeneity. The focused power of the laser beam was also checked for each wavelength to avoid any transformation or heating of the samples. Accordingly, the power was kept below 100 µW and the magnitude X50 of the objective has been selected after a test list. The confocal mode was also sometimes used to select a smaller analysed volume in the same irradiated volume. This measurement was perfomed by Prof. Bernard Humbert from IMN (Institut des Matériaux de Nantes).

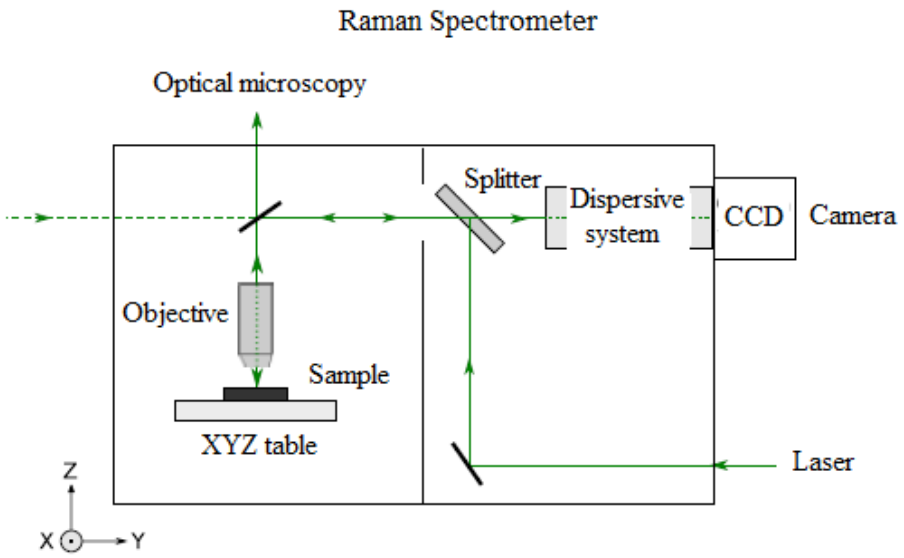

Figure 17. Schematic configuration of Raman spectrometer at the IMN

2.6. Non-linear sum-frequency generation spectroscopy setup

Based on home-made SFG system at Institute of Physical Chemistry, Orsay, the acquisition of SFG spectra was performed by utilizing an IR laser source (Nd:YAG, 1064nm, 12ps) coupled with an acousto-optic modulator (100MHz micropulse repetition rate, 2μs train, 25Hz macropulse repetition rate). There are two different Optical Parametric Oscillators (OPO). The infrared OPO with wavelength used over the spectral range from 3.3μm to 3.6μm while the visible OPO is tunable over 450nm to 650nm. To obtain an SFG signal, the five fixed visible (475nm, 500nm, 527nm, 570nm, and 600nm) and tunable infrared beams must be coherently mixed, temporally and spatially, at the same point of the sample surface. There are two types of linear polarizations: S and P. By convention, the notation of polarization configuration is defined in the increasing order of wavelength: (SFG,VIS,IR). The polarization of the infrared beam is fixed by the source (P) and remains unchanged. It is recommended that the polarization configuration for gold (Au) sample is PPP while the suitable configuration for glass sample is SSP (Figure 9). The explanation for this choice is related to the nature of refractive index of substrate or mathematically related to surface reflectivity properties. Gold material possesses higher reflectivity than glass, so the glass sample will be analyzed in SSP configuration. The SFG beam was collected by photomultipliers after using filters and monochromator to filter spatially and spectrally.

3. RESULTS AND DISCUSSION

3.1. Optoelectronic properties of QDs

To investigate the optoelectronic properties of QDs grafted on glass substrate, UV-VIS absorption and Fluorescence emission spectroscopies are taken into consideration. To evidence the success of chemical deposition process of different QDs on glass, the presence of QDs on glass will be detected through spectral identification in comparison with colloidal QDs' absorption spectra.

3.1.1. UV-VIS spectroscopy

3.1.1.1. Absorption spectra of colloidal QDs

The spectra of the first excitonic states of three different colloidal QDs are presented in Figure 18. It can be seen that the first excitonic absorption peak is positioned at 484 nm, 535nm, and 567nm for QD520, QD570, and QD610 respectively. The locations of first absorption peaks of both QD520 and QD610 are close to the values published from previous study [21] which are 488nm for QD520 and 566nm for QD610. The reason for the small variation of these peak locations can be rooted from the discrepancy of density of QD in colloidal solutions. In previous study, the density was 3.66×10^{20} m^{-3} for QD520, and 1.47×10^{20} m^{-3} for QD610 while the QD density is theoretically $N = 3.0 \times 10^{20}$ m^{-3} (in 0.5μM QD solutions) in this study.

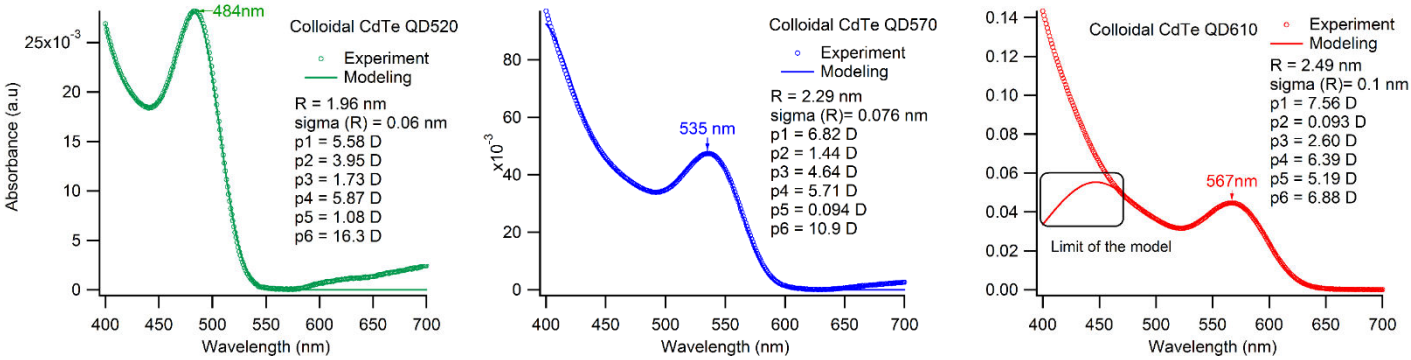

Figure 18. UV-VIS absorption spectra of different colloidal QDs solutions and their corresponding fitting results

Applying Igor Pro software to modelize the absorption spectrum of QDs, the fitting procedure is based on equation (6) and the fitting lines are also depicted in Figure 18. In this procedure, the variables directly affecting the fitting consists of 10 parameters: colloidal QD concentration N, optical pathway ℓ, QD radius R, radius standard deviation $\sigma(R)$, and six dipole moments of the first sixth excitonic states $p_{1\to6}$. Amongst them, the values of N and $\ell = 0.01$m are known and the values of 6 dipole moments are deduced from reference values from previous study [20, 22]. Hence, only two parameters taken into consideration are radius of QD (R) and its standard deviation $\sigma(R)$ in the fitting procedure. During fitting, the known values remain unchanged while other parameters are first manually defined and then automatically fitted to obtain the best fitting line. Functionally, the fitting of radius of QD determines the position of the peak. Otherwise, the other parameters define the peak intensity and peak width.

The values of fitting parameters are collected and given in each spectrum corresponding to different QDs. The extracted values $R \pm \sigma(R)$ of QD520, QD570, and QD610 are 1.96 ± 0.06 nm, 2.29 ± 0.08 nm, and 2.49 ± 0.10 nm. It is clear that the tendency of the size of QDs raises with the increasing position of the peak. This conclusion supports the quantum confinement effect stated in the first section of this report. Due to the decrease of QD's size, the blue shift occur in both absorption and emission spectrum. From HR-TEM measurements, the average diameters of QD520 (3.4 ± 0.6 nm) and QD610 (3.8 ± 0.7 nm) were proved [21]. In comparison with the values from Igor Pro fitting, there is an anology between experimental data and evaluated fitting data. Furthermore, the confidence interval of QDs' size in fitting is higher than the one from HR-TEM measurements. HR-TEM measurements are based on a

maximum of 40 single QDs, which gives poor statistics. Meanwhile, UV-VIS spectroscopy probes a huge number of QDs within the solution. Hence the statistics is much better.

From the fitting lines of three UV-VIS absorption spectra, the absorption peaks of QD520 and QD570 are well-fitted without the appearance of the second excitonic peak. However, this phenomenon is seen in the case of QD610. The mismatch from the latter (lower wavelength) can be attributed to the limit of the fitting model which is based on a finite number of excitonic states of QDs. As the size of QDs increases, it seems that taking the first six excitonic states of QDs into account does not suffice to modelize the absorption spectrum. Therefore, the model failed for QD610 to describe the first part of the absorption spectrum.

3.1.1.2. Absorption spectra of QDs monolayers samples

Considering the QD monolayer samples deposited on glass substrate, Figure 19 depicts the first excitonic spectrum of different QDs on glass with their corresponding fitting lines by Igor Pro. The maximum absorbance of these QDs are measured: at 477nm for QD520, at 534nm for QD570, and at 562nm for QD610. It can be seen that there is a small shift (less than 10 nm) for QD 520 (Δ_λ= 7nm), for QD610 (Δ_λ= 5nm) compared to corresponding spectra in colloidal solutions. To be particular, all kinds of QDs deposited on glass via APTES linking agent absorb UV-VIS light at a smaller wavelength than colloidal QDs. It can be deciphered by the change of chemical environment. Moving from colloidal QDs with water solvent to QD's monolayer grafting on glass, the absorption bands expect such a small changes just due to the fact that the medium has changed, from aqueous solution to solid substrate and QDs are in closer contact.

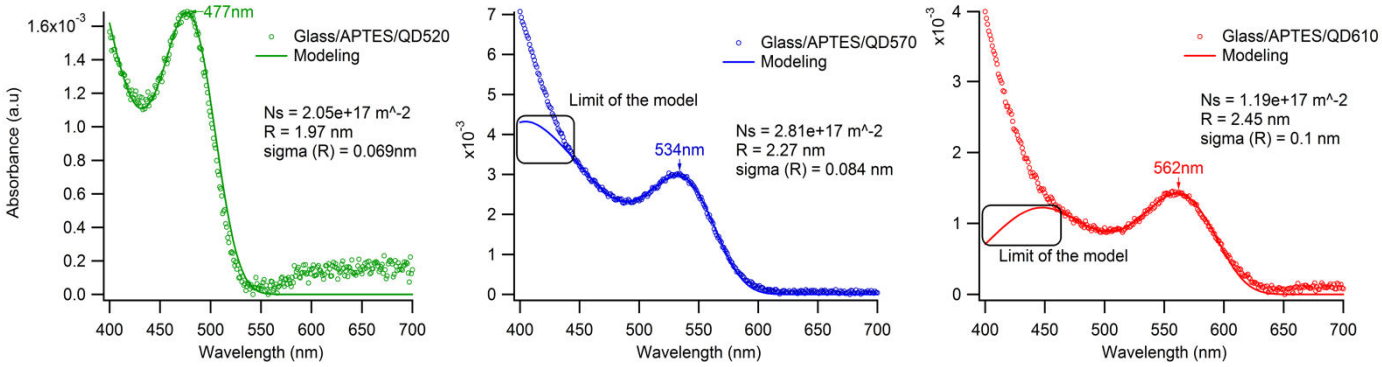

Figure 19. UV-VIS absorption spectra of different QDs monolayers samples and their corresponding fitting results

As previously stated, instead of using concentration N and optical pathway ℓ in fitting procedure, the QD's density N_s on the surface of glass substrate will be the determining parameter and the fitting procedure is based on equation (7). Other parameters are mainly based on the values from fitting procedure on colloidal QD solutions and kept fixed during fitting. The N_s and radius $R \pm \sigma(R)$ parameters were released until achieving the best-fit values during the invariation of other parameter's values. Then they were fixed one by one. The fitting values are stated in Figure 19: $N_s(\text{QD520}) = 2.05 \times 10^{17} m^{-2} = 0.205\, nm^{-2}$, $N_s(\text{QD570}) = 2.81 \times 10^{17} m^{-2} = 0.281\, nm^{-2}$, $N_s(\text{QD610}) = 1.19 \times 10^{17} m^{-2} = 0.119\, nm^{-2}$.

With the chemical protocol we used, we grafted QDs on both sides of the glass slide. So, in reality, we have to divide N_s by 2 to get the real surface density on a single side of the glass substrate. Besides, the theoretical surface density of a closed-packed QD monolayer is ${N_s}^o(1 \text{ layer}) = \frac{1}{D^2}$ where D is the diameter of QD (nm). The number of QD layers on the glass samples is calculated by $n = \frac{{N_s}'}{{N_s}^o}$ and is summarized in Table 2. From these calculations, it can be seen that we grafted QD520s a bit more than a monolayer, but less than a bilayer ($1 < n < 2$) which is fairly good. However, 2.9 layers for QD570 and 1.4 layers for QD610 have been noticed on glass sample. To conclude, the QD610-grafted sample is closer to the ideal case of a monolayer than the two others.

Table 2: The estimated number of QD layers on the samples (n)

QD-deposited sample	N_s' (single side) (nm^{-2})	N_s^o(1 layer) (nm^{-2})	$n = \frac{N_s'}{N_s^o}$
QD520	0.103	0.065	1.6
QD570	0.141	0.049	2.9
QD610	0.060	0.043	1.4

The limitation of fitting procedure was recognised in both QD570- and QD610-grafted samples. The elucidation of this observation is also from the false consideration of the finite number of QD's excitonic states on fitting procedure. Due to the weaker intensity of absorption spectra than in colloidal solutions, the fitting are even more challenging for QD570 and QD610.

3.1.2. Fluorescence spectroscopy

3.1.2.1. Emission spectra of colloidal QDs

The fluorescence emission peaks of colloidal QDs are measured at: 520 nm for QD520, 570nm for QD570, and 605nm for QD610 (Figure 20). These values are similar or in the range of emission wavelength stated by Sigma-Aldrich manufacturer (QD520: 520 ± 5nm, QD570: 570 ± 5nm, QD610: 610 ± 5nm) as well as other papers [21, 22] .

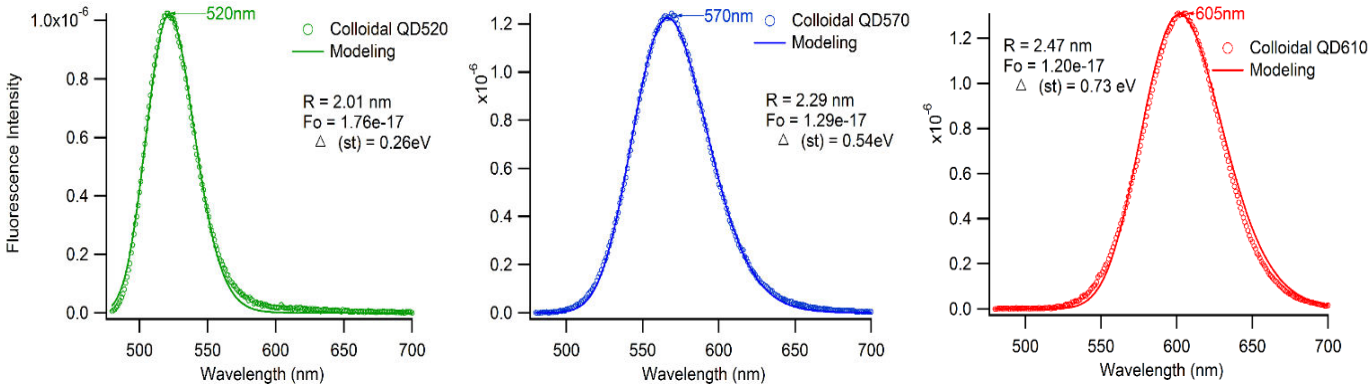

Figure 20. Fluorescence emission spectra of different colloidal QDs solutions and their corresponding fitting results

As far as the fitting procedure is concerned, the variation of the amplitude F_o, the Stokes shift $\Delta_{St.}$ are adjusted to acquire the best fit. Other variables in equation (10) are refered to UV-VIS fitting. The values of these predominant factors in fluorescence fitting for each colloidal QD solution are indicated in Figure 20. In general, the radius of each type of QD is closely consistent to the values from absorption fitting (with small variation of 0.01-0.03nm) and the amplitudes F_o value of three QDs are around 10^{-17}. The Stokes shifts $\Delta_{St.}$ are compared with the other previous studies: QD520 ($\Delta_{St.}$= 0.15eV) and QD610 ($\Delta_{St.}$= 0.13eV) [20, 21]. The difference between the values of this report and published values can be ascribed to (1) chemical reason - the difference of colloidal QD's concentration and (2) technical reason - the range of data fitting. As discussed in section 3.1.1, the variation of colloidal QD520's concentration between two investigations is smaller with respect to the case of QD610 (approximately double the concentration of QD610 in ref. [21]). Hence, the discrepancy of $\Delta_{St.}$ values in case of QD610 is also more significant. Secondly, it is recognisable that the fitting range of QDs in this report is not as ideally even between two tails of data as the one in the previous study.

3.1.2.2. Emission spectra of QDs monolayers samples

In terms of QD-deposited glass samples, the fluorescence maximum is located at 512nm for QD520, 576nm for QD570, and 606nm for QD610 (Figure 21). Compared to emission wavelengths extracted from corresponding colloidal solutions, there are some notifications. For QD520, the spectrum of fluorescence of QD-deposited glass sample is

blueshifted compared to colloidal QD ($\lambda_{emission}$ = 520nm). This observation can be ascribed to differences in structure and assembly of QDs on glass substrate and in solution. On glass substrate, QD520s form a monolayer and the fluorescence light is collected from single QD520 without encountering any close neighbor QD520 because there are no thick stacks of QD520s. In solution, the light emitted by a given QD520 propagates through the colloidal QD520 solution along the optical pathway to the detector, so that the light may encounter other QD520s in solution and be reabsorbed before being detected. Given the spectral overlap between the absorption and emission spectra of QD520, the short-wavelength part of the emission band is partially absorbed (and not detected) in colloidal solution. Therefore, the spectrum of QD520 monolayers appears blueshifted with respect to colloidal QD520 solution.

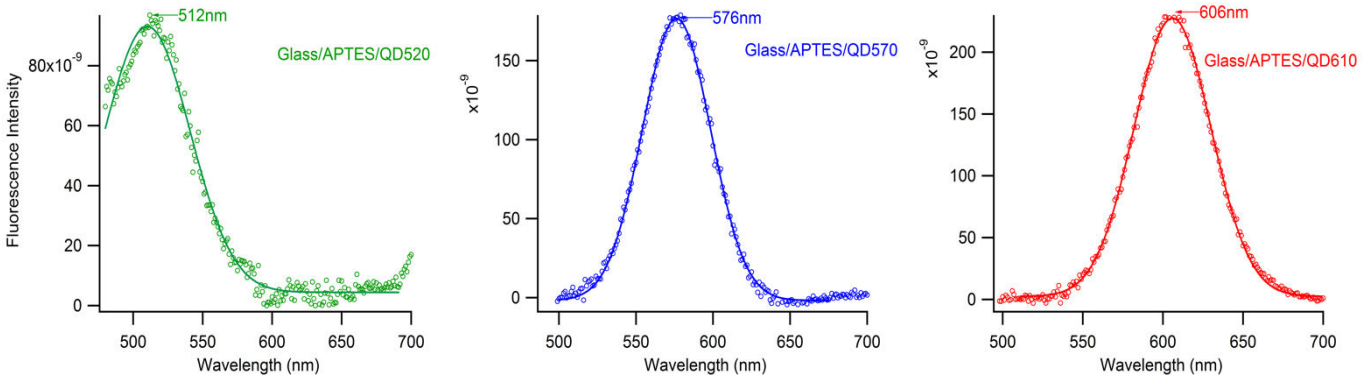

Figure 21. Fluorescence spectra of different QDs monolayers samples and their corresponding fitting results

In case of QD570, the emission spectrum of QD-deposited glass sample is significant redshifted (λ_{QD570} = 576nm). We can deduce that the structure of QDs on glass substrate is not strictly monolayer. This is compatible with our estimation of the number of layers in section 3.1.1.2 from UV-vis spectroscopy: as deduced from N_s, QD570-grafted sample is probably made of 3 QD layers. Hence, the redshift of 6 nm can be explained by some stacks of QD layers enabling QD570s to couple through homo-Förster Resonant Energy Transfer (FRET) when they are almost in contact on glass substrate. Within the same QD population, the smallest QDs (emitting at a small wavelength - donor) transfer their energy to the biggest QDs (emitting at a large wavelength – acceptor). Hence, there is a lost of energy of the "blue" side of the emission spectra, to the benefit of the "red" side and the redshift has appeared. QD610-deposited substrate does not experience a significant redshift (λ_{QD610} = 606nm on glass, with respect to 605 in solution). This is consistent with the fact that this sample is the closest to the ideal case of a monolayer. We estimated from N_s a number of 1.4 layers.

The modeling for QD-grafted glass samples is based on Gaussian function approximation. It is noticable that there is a slight discrepancy between the shape of the experimental spectra and modeling line, especially QD520. The interpretation of this observation may be imputable to the size distribution of QDs is not perfectly Gaussian. It is assumed that the idealized model of QDs shape is perfectly spherical but it is not the case as deduced from HR-TEM result [20, 21].

3.1.3. Time-resolved Fluorescence Spectroscopy

Time-resolved measurements of the fluorescence emitted by colloidal QD520, QD570, and QD610 (left) and their corresponding QDs on glass substrates (right) is shown in Figure 22. The fitting lines are obtained by a multi-exponential model by considering three (for colloidal QDs) or four (for QDs-grafted glass samples) populations of QDs with different lifetimes τ_n (expressed in nanoseconds) (equation (11)). The histograms indicate the statistical distribution of the lifetimes, deduced from the amplitudes A_n in percentage (y-axis) and the lifetimes τ_n in ns (x-axis). From equation (12), the average lifetime is calculated and given in Table 3.

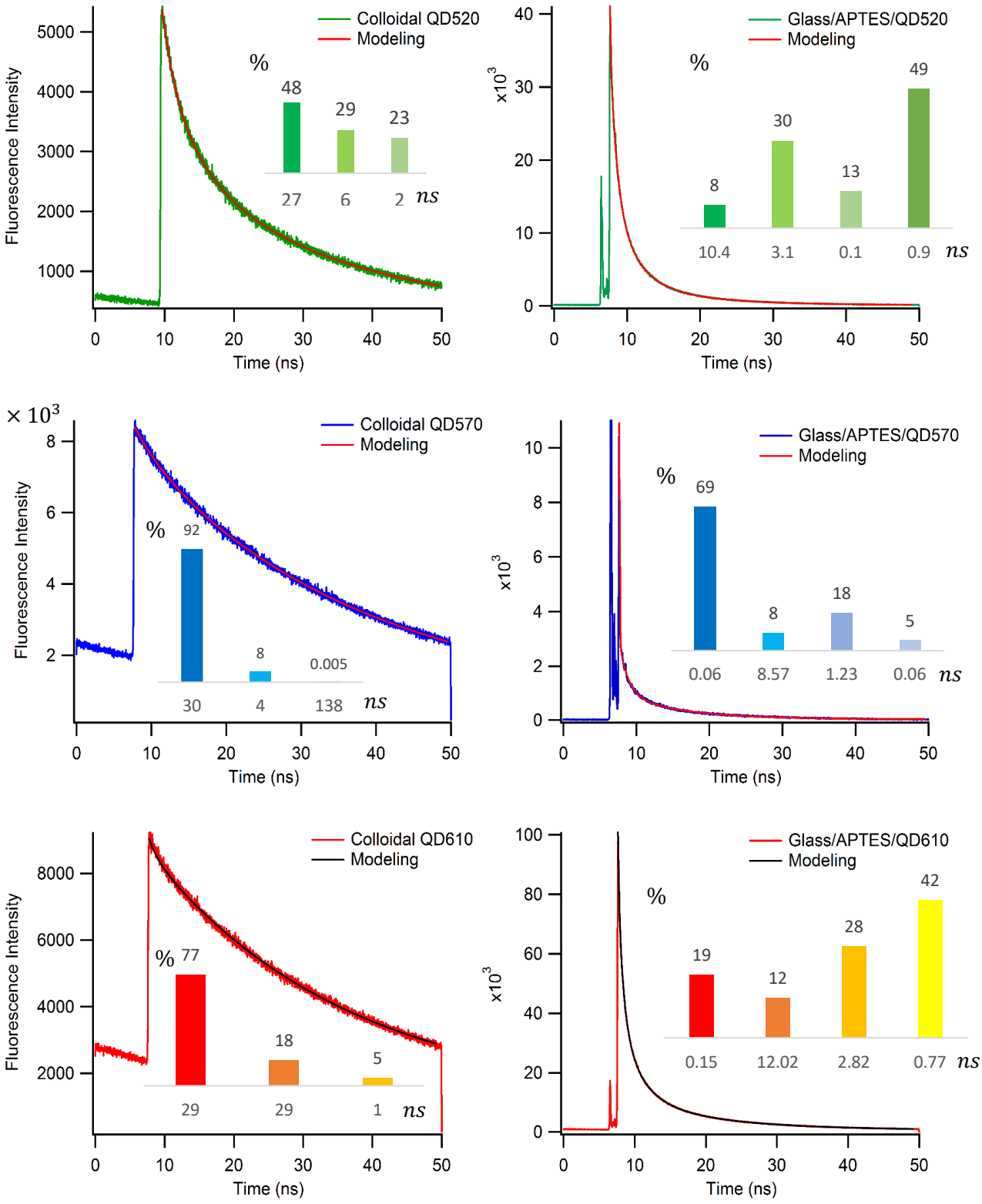

Figure 22. Exponential data modeling of the fluorescence decays of colloidal QDs (left) and corresponding QD-grafted glass sample (right) with each lifetime's percentages illustrated in histogram.

Table 3: Caculated average lifetime of different QDs in colloidal solutions and QD monolayer samples

Type of QD	$\tau_{n_{ave}}$(colloidal QDs) (ns)	$\tau_{n_{ave}}$(QD monolayers) (ns)
QD520	15	2.2
QD570	28	1.0
QD610	27	2.6

It is obvious that all kinds of QDs in colloidal solutions experienced a much slower quenching effect of fluorescence in relation to QD's monolayers on glass ($\tau_{n_{ave}}$(colloidal

QDs) $\gg \tau_{n_{ave}}$(QD monolayers)). It can be interpreted by the appearance of aggregation effect of QDs on the surface of glass substrate. QDs in monolayers might be stuck together and accumulated to form some QDs aggregation. In addition, the quenching can also be due to the molecular interactions between APTES with positive charges from -NH_3^+ groups and the QD ligands with negative charges from -COO^- groups. Nonetheless, QDs in colloidal solutions are electrostatically repulsive and isolated because of no attractive interaction [22].

3.2. Charaterization of chemical structure of QD monolayers on glass

Even though we performed Raman and SFG measurements on all three different QDs monolayers (QD520, QD570, QD610) during this internship, we will here focus our discussion on the Raman and SFG analyses made for QD570 only, which will serve as a representative for the explanation about chemical structure and energy transfer between QD monolayer and APTES monolayer.

3.2.1. Raman spectroscopy

From Raman spectrum of QD570 monolayer on glass with three different excitation wavelengths (488nm, 514nm, and 633nm) (Figure 23), there are several noticeable features. The vibrational fingerprint ranges from 0 to 4000 cm^{-1} and Raman peaks are remarkably seen at excitation wavelengths of 488 nm and 514 nm. The assignment of Raman signals is determined from 2800 to 3100 cm^{-1} of Raman shift (Figure 23b) in order to correspond with SFG spectral range which will be presented in next section and is detailed in Table 4.

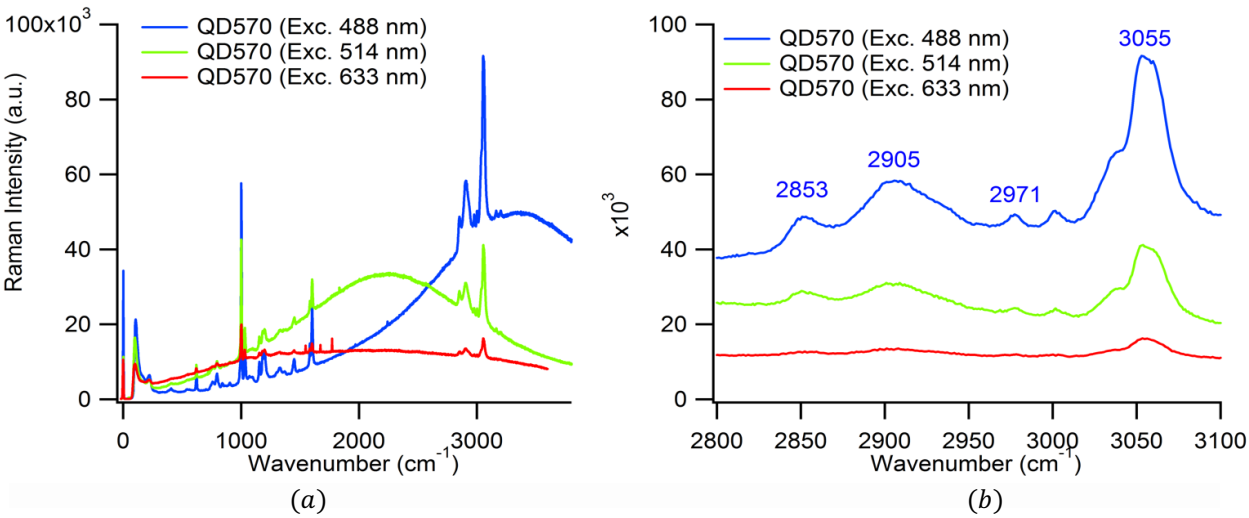

Figure 23. Raman spectra of QD570 monolayers sample with three different excitation wavelengths (left) and the corresponding expansion of Raman spectrum in the range of 2800-3000 cm^{-1} (right)

Table 4: Vibrational mode assignment of QDs monolayer on glass samples in Raman spectroscopy

Peak position (cm^{-1})	Spectroscopic notation	Vibrational mode	Reference
2853	$\nu_s(NCH_2)$	-CH_2- symmetric stretching	[28]
2905	$\nu_a(NCH_2)$	-CH_2- asymmetric stretching	[28]
2971	$\nu_a(CH_3)$ and $\nu_s'(CH_3)$	-CH_3 asymmetric stretching	[28]
3055	$\nu_a(NH_3^+)$	-NH_3^+ asymmetric stretching	[29]

From the Raman vibrational fingerprint library of APTES, the vibrational modes (2853 and 2905 cm^{-1}) of -CH_2- which is closest to amine group and the vibrational mode of -CH_3 in -OCH_2CH_3 head (Figure 11) are noticed in Raman spectra of QD570-grafted glass sample. Interestingly, the stretching mode of protonated amine group (NH_3^+) is predominantly intense among all the Raman peaks at 3055 cm^{-1}. Therefore, it suggests that the electrostatic interactions between QDs and APTES molecules has been established from chemical protocol.

Although the Raman signals mentioned above mainly come from APTES molecular structure, there are some recognitions for the peaks of mercaptopropionic acid-coated QDs in

the lower Raman shift region. At 620 and 794 cm^{-1}, these two peaks are assigned to the C-S streching mode of mercaptopropionic acid molecule (Figure 11). In comparison with pure mercaptopropionic acid solution, these two peaks are located at 671 and 763 cm^{-1} [30]. The observed shift can be attributed to the electron withdrawal characteristic of S-CdTe bondings to the C-S bonds in mercaptopropionic acid molecules [31]. Besides, two Raman bands at 1453 and 1602 cm^{-1} may be appointed to the vibrations of non-dissociated carboxyl group (the combination of C-O stretching with O-H bending and C=O stretching, in turn) [32]. The corresponding vibrations (at 1422 and 1657 cm^{-1}) are also collected from Raman spectrum data of mercaptopropionic acid solution [30]. This shift might be related to the pH effect to the dissociation of carboxylic group -COOH between pure acid solution and coated QDs on glass.

Furthermore, the baseline from Raman spectrum of QD570 monolayer on glass is not constant because we observed a broad band, and its location depends on the excitation wavelength. In order to interpret this observation, spectra with Raman intensity versus wavelength are plotted by a simple unit conversion as follows:

$$\Delta\omega = \frac{10^7}{\lambda_{excitation}} - \frac{10^7}{\lambda} \Leftrightarrow \frac{1}{\lambda} = \frac{1}{\lambda_{excitation}} - \frac{\Delta\omega}{10^7} \Leftrightarrow \lambda = \frac{1}{\frac{1}{\lambda_{excitation}} - \frac{\Delta\omega}{10^7}} \qquad (14)$$

where $\Delta\omega$ is Raman shift (cm^{-1}), wavelength λ (nm), excitation wavelength $\lambda_{excitation}$ (nm).

Regarding Figure 23a, for an excitation wavelength of 488nm, there is a broad band around Raman shift of ~2950 cm^{-1} (blue spectrum) and it shows that the Raman wavelength corresponds to 570 nm which is the maximum of the QD fluorescence emission. It can be seen that a similar effect with the excitation wavelength of 514 nm and a Raman shift of ~1911 cm^{-1} (green spectrum). The Raman wavelength conversion is also consistent with the maximum of the QD570 fluorescence emission.

For the purpose of confirming the Raman results with fluorescence spectrum of QD570, a Raman spectrum in wavelength (nm) has been generated based on equation (14) and is illustrated in Figure 24.

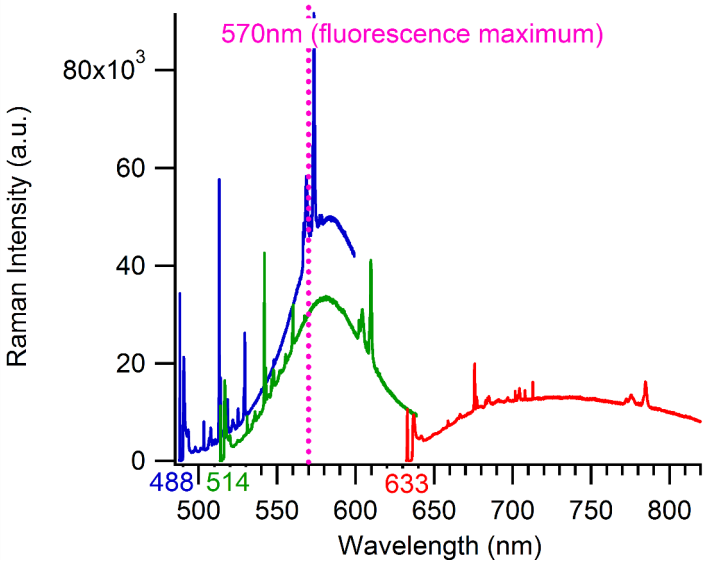

Figure 24. Raman spectra conversion from wavenumber (cm^{-1}) to wavelength (nm).

As can be noted from Figure 24, the existence of peak which covers the fluorescence maximum at 570nm in the spectrum of 488 and 514nm excitation. That fortifies the coherence of fluorescence emission results and Raman analysis about the establishment of QD570 monolayer on glass substrate. Otherwise, there is no peak in the case of 633nm excitation. When we use a laser at 488 or 514 nm, we excite the QDs because they absorb the light at these wavelengths. As a consequence, QDs emit their fluorescence at 570 nm and we see it in the Raman spectra. But when we use a laser at 633nm, it is not absorbed by the QD570s, which

are transparent at this wavelength. This is why we don't see any contribution of the QD fluorescence in the Raman spectrum with the excitation at 633 nm.

3.2.2. Non-linear sum-frequency generation spectroscopy

To account for the data of SFG, the fitting procedure needs proceeding. Theoretically, the intensity of the SFG beam is proportional to

$$I(\omega_{SFG}) \propto \left|\vec{E}_{(\omega_{SFG})}\right|^2 \rightarrow I(\omega_{SFG}) \propto \left|\vec{P}_{(\omega_{SFG})}\right|^2$$

and then, $I(\omega_{SFG})$ can be expressed by [20, 23, 25]:

$$I(\omega_{SFG}) = \frac{8\pi^3 \omega_{SFG}^2 sec^2\theta_{SFG}}{c^3 n_{air}(\omega_{SFG}) n_{air}(\omega_{IR}) n_{air}(\omega_{VIS})} || \chi_{interface}{}^{(2)} ||^2 I_{IR} I_{VIS} \quad (15)$$

Considering the surface reflectivity (neglecting the Fresnel factors), the effective second order susceptibility can be expressed by equation (16). It is a combined contribution of the inorganic components of the samples (glass slide and CdTe core) ($Ae^{i\varphi}$) and the remaining part from organic components (APTES or mercaptopropionic acid functionalized on QDs).

$$\chi_{interface}{}^{(2)} = \chi_{substrate}{}^{(2)} + \chi_{adsorbate}{}^{(2)} = Ae^{i\varphi} + \sum_v \frac{a_v e^{i\psi_v}}{\omega_{IR} - \omega_v + i\gamma_v} \quad (16)$$

where A is the contribution of amplitude of the background, φ is the phase of the background, v is the index of peaks, a_v is the amplitude of the v^{th} peak, ω_v the position of the v^{th} peak (in cm^{-1}), ψ_v is the phase of the v^{th} peak which is assumed to be zero for simplicity, and γ_v is the ½ width at half height of the v^{th}peak (in cm^{-1}) (or damping constant). The fitting lines are associated with experimental data in Figure 25.

Indeed, the particularity of the SFG setup of the ICP, Orsay is its capacity to be able to change the wavelength of the infrared and the visible. This feature is remarkable because it allows us to maximize the intensity of the SFG beam, using the visible wavelength corresponding to a UV-VIS absorption peak. Regardless of the excitation wavelengths of visible beam (475nm, 500nm, 527nm, 570nm and 600nm), 5 SFG spectra are carried out on the same sample, under the same conditions in Figure 25a,b,c,d,e. The spectral range with our SFG data on QD570 is located in the 2800-3000 cm^{-1} region. To be specific, the QD570s have their absorption peak at 535nm in colloidal solution and at 534nm for our sample (Figure 18 and Figure 19). The peaks correspond to the first excitonic state (Figure 7). It is easily noticed that the intensity of the SFG beam is close to the maximum for an input visible wavelength of 527 nm (Figure 25c). In addition, one can also relate the other incidence visible wavelengths to the absorbance spectrum (Figure 25f): 600nm corresponds to an absorbance close to 0 while 570nm corresponds approximately to the intensity at half height (of the first peak) and 475nm and 500nm corresponds to the local minimum between the first and the second peak (this last second peak is not technically detectable due to the technical limit of spectrometer).

It can be seen that on each of the five SFG spectra, four molecular vibrational modes (2855, 2885, 2912, and 2947 cm^{-1}) are observed (Figure 25). Based on references [23, 33], the peaks at 2855 cm^{-1} and 2912 cm^{-1} correspond to the stretching modes of methylene (-CH_2-): the symmetric and asymmetric stretching vibration modes, respectively. It can be rooted from methylene of organic ligands (HS-$(CH_2)_2$-COOH) of QDs and APTES molecules grafting QDs $(CH_3CH_2O)_3Si(CH_2)_3NH_2$. The maximum of SFG signal at 2912 cm^{-1} for all spectra proves that the combined effect of -CH_2- in both organic ligand and APTES amplifies the SFG intensity. The presence of methyl -CH_3 group is indicated by a symmetric mode at 2885 cm^{-1} [23, 33]. The presence of methyl could potentially be ascribed to the APTES used for the silanization of glass slides. Otherwise, -CH_3 might be possibly from a residual part of an organic solvent compound used in the QD monolayer preparation protocol such as CH_3OH, CH_3CH_2OH. Another possibility would be an inaccuracy in the composition of stock QD solutions from our supplier. Although low amplitudes of the last peak at 2947 cm^{-1}, it could be referred as a vibration of asymmetric stretching mode of -OCH_2- from APTES [28].

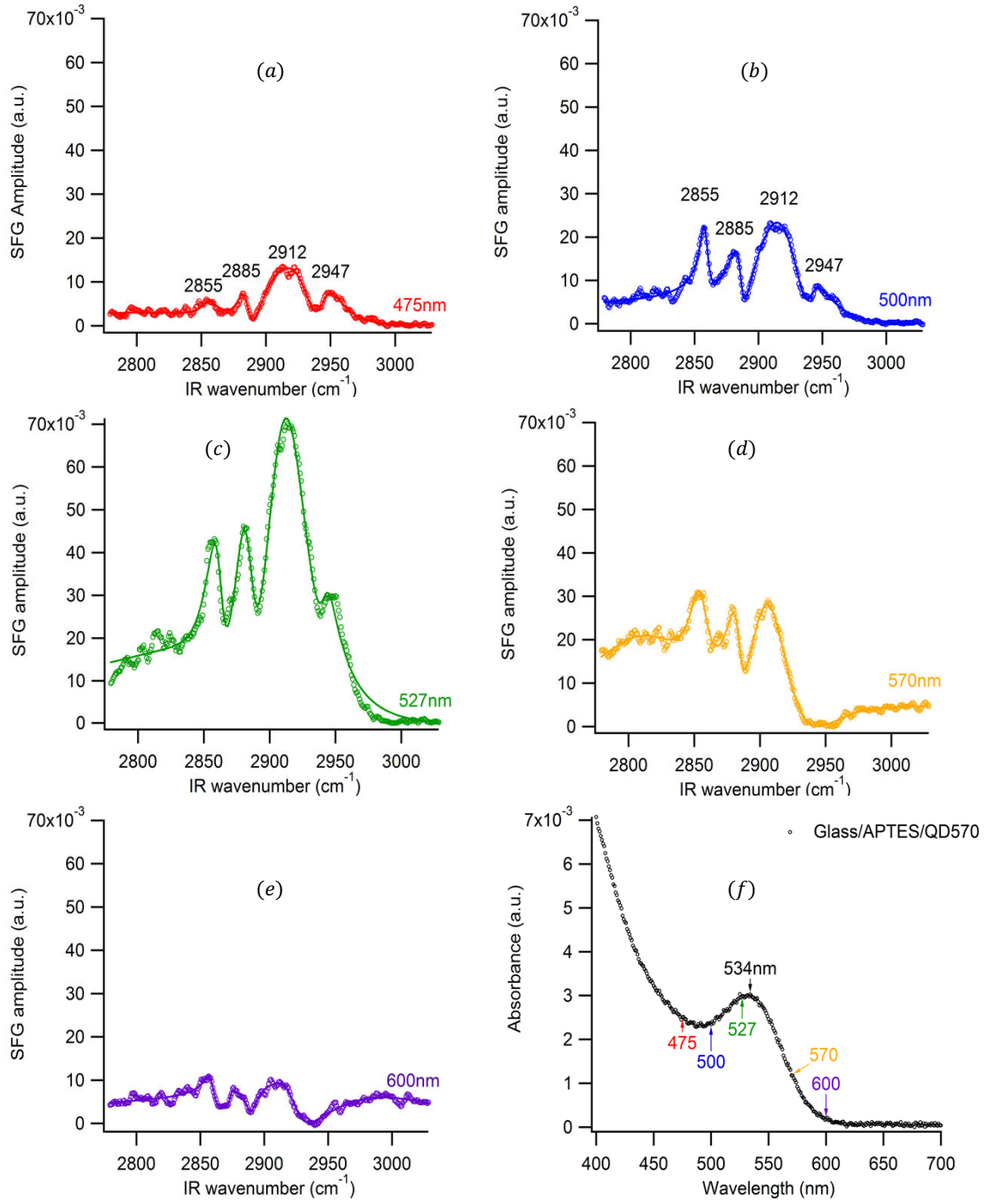

Figure 25. SFG spectra of QD570 monolayers sample at different visible excitation wavelengths and the corresponding fitting line (a,b,c,d,e) and the UV-VIS absorption of sample is in f) to locate the five visible wavelengths.

From SFG peak analysis, these vibrations are maximally amplified by the energy transfer between the QDs and their organic ligands as well as grafting molecules APTES for a well-defined input visible wavelength at 527 nm in Figure 25c. Under the effect of the excitation induced by the visible beam, excitons transfer part of their energy from the core of the QDs by dipolar coupling (Figure 2b) to not only the organic acid ligands but also the entire chemical environment including anchoring agent APTES attaching QDs on glass substrate. The energy of these excitons leads to the amplification of the intensity of the vibrations of the close molecule neighboring (APTES + organic ligands) observed by SFG spectroscopy. Finally, we observe that the difference in SFG amplitude with visible wavelengths (475, 500, 570, and 600nm) in relation to the SFG amplitude obtained with a visible wavelength of 527

nm dominantly follows the absorption spectrum (Figure 25f). Hence, the SFG analysis emphasizes the dipolar coupling from excitons to ligand as well as grafting molecule vibration which is crucial to improve the detection threshold in nanosensors based on QDs.

3.3. Difficulties and recommendations

During my internship, there are several issues related to the nanosensor performance efficiency that I have experienced. It leads to some losses in optical properties of QD samples when transferred from solution to glass as well as chemical characterizations later on. The most common issues during my internship stem from the procedure of chemical protocol for experiments. I hereafter indicate some difficulties:

(1) Due to the desired protocol of monolayers assembly of both APTES and QDs on glass substrate based on physisorption strategy (electrostatic interaction), the process of grafting is the trickiest step. Due to the synthesis of APTES monolayer which needs discarding the multilayer of APTES during 1.5h physisorbed on glass, the multilayer removal step must work under sufficient sonication. During my two-week internship in Liège, the ultrasonic waves of sonicator might have been too rigorous, so there are some chances that the assembly of APTES on glass samples could be destroyed. Thus, some of QDs' samples are weird and less intense in absorption spectrum. Besides, the polymerization of APTES can be occured if there are any traces of water molecules on glassware from the beginning or during rinsing steps with MeOH. Practically, the white traces of polymerized APTES were seen by eyes and those samples were discarded.

(2) The step of removing stacks of QDs to get QDs monolayer should be under water rinsing with medium flow. With strong water rinsing flow, the deposition can be damaged due to the APTES-QD bonding breaking. At first, I applied a strong flow of MilliQ water in the last step, there was no QDs absorption band in UV-VIS spectrum.

(3) During the synthesis, N_2 drying step also brought some serious issue to graft QDs on glass. It is recommended that drying with N_2 should be mandatory performed before air drying itself, especially during cleaning steps with organic solvents. Furthermore, I usually experimented several glass samples simultaneously so to make sure the protocol done perfectly is also reproducible.

(4) Conditions for experiments and storages: Due to the nature of physorption strategy of QD coated with COOH and APTES, the temperature effect is taken into account. It is suggested that the experiment should be conducted in the laboratory with 22 ^{o}C tempature or room temperature. Sample's storage also follows this recommendation. For instance, the temperature control during the transportation of QD samples to Liège is alo quite challenging for me to keep the stability of QD monolayer samples.

CONCLUSIONS AND FURTHER STUDY

In this report, a thorough study about optical properties and vibroelectronic interation of different COOH-functionalized CdTe QDs (QD520, QD570, and QD610) deposited on glass substrate via anchoring agent APTES has been investigated. Based on all above discussions, QD's absorption and emission studies prove that we succeeded in transferring very well the optoelectronic properties of QDs from colloidal solution to solid substrate without degradation. The very good efficiency of chemical deposition protocol for grafting QDs on glass through electrostatic interaction with APTES molecules has been noticed from absorption and emission studies. From Raman and SFG analyses, we shew the existence of vibroelectronic coupling between QDs and the surrounded organic ligands as well as further APTES grafting molecules. The novelty of this research report is the successful establishment of QD monolayer on glass substrate as nanosensor model for detection threshold improvement. However, the confirmation from theoretical study such as density of state for single QD-based nanosensors should be investigated. Furthermore, the further study should consider FRET-based sensors for which QDs are both donors and acceptors for the detection of biological interactions.

REFERENCES

1. Ahmed AH Abdellatif, M.A.Y., Mansour Alsharidah, Osamah Al Rugaie, Hesham M Tawfeek, *Biomedical Applications of Quantum Dots: Overview, Challenges, and Clinical Potential.* International Journal of Nanomedicine, 2022. **17**: p. 1951-1970.
2. Juan Hu, Z.y.W., Chen-chen Li, and Chun-yang Zhang, *Advances in single quantum dot-based nanosensors.* Chemical Communications, 2017. **52**: p. 1-13.
3. Brkić, S., *Applicability of Quantum Dots in Biomedical Science.* IntechOpen, 2018: p. 21-39.
4. Alireza Valizadeh, H.M., Mohammad Samiei, Samad Mussa Farkhani, Nosratalah Zarghami, Mohammad kouhi, Abolfazl Akbarzadeh, Soodabeh Davaran, *Quantum dots: synthesis, bioapplications, and toxicity.* Nanoscale Research Letters, 2012. **7**(480): p. 1-14.
5. Adriana Fontes, R.B.d.L., Maria Aparecida Barreto Lopes Seabra, Thiago Gomes da Silva, Antônio Gomes de Castro Neto and Beate Saegesser Santos, *Quantum Dots in Biomedical Research.* IntechOpen, 2012(269-290).
6. Muthupandian Ganesan, P.N., *Quantum Dots as Nanosensors in Detection of Toxics – A Literature Review.* Royal society of Chemistry, 2020. **10**: p. 1-21.
7. Angela M. Wagner, J.M.K., Gorka Orive, Nicholas A. Peppas, *Biomedical Applications of Quantum Dots: Overview, Challenges, and Clinical Potential.* Acta Biomaterialia, 2019. **94**: p. 44-63.
8. Chun-Yang Zhang, H.-C.Y., Marcos T. Kuroki, Tza-Huei Wang, *Single-quantum-dot-based DNA nanosensor.* Nature materials, 2005. **4**: p. 826-831.
9. Julie Hottechamps, T.N., Alain Brans, Christophe Humbert, and and L. Dreesen, *How Quantum Dots Aggregation Enhances Förster Resonant Energy Transfer.* ChemPhysChem, 2020. **21**: p. 853-863.
10. Knoss, R.W., *Quantum Dots - Research, Technology and Applications*. 2008: Nova Science Publishers
11. Hartmut Haug, S.W.K., *Quantum Theory of the Optical and Electronic Properties of Semiconductors*. 5 ed. 2009: World Scientific.
12. Edvinsson, T., *Optical quantum confinement and photocatalytic properties in two-, one- and zero-dimensional nanostructures.* R Soc Open Sci, 2018. **5**(9): p. 180387.
13. Gaponenko, S.V., *Optical Properties of Semiconductor Nanocrystals*. Cambridge Studies in Modern Optics. 1998: Cambridge University Press.
14. Yoffe, A.D., *Semiconductor quantum dots and related systems: Electronic, optical, luminescence and related properties of low dimensional systems.* Advances in Physics, 2001. **50:1**: p. 1-208.
15. Sergey V. Gaponenko, H.V.D., *Quantum confinement effects in semiconductors*, in *Applied Nanophotonics* 2018, Cambridge University Press. p. 52 - 91.
16. Gopal Ramalingam, P.K. and T.E. Ganesan Ravi, Bojarajan Arjun kumar, Nadarajah Manivannan and Kaviyarasu Kasinathan, *Quantum Confinement Effect of 2D Nanomaterials.* IntechOpen, 2020.
17. Wagner, A.M., et al., *Quantum dots in biomedical applications.* Acta Biomater, 2019. **94**: p. 44-63.
18. Rao CNR, Cheetham AK., *The Chemistry of Nanomaterials: Synthesis, Properties and Applications*. 2004: Wiley-VCH.
19. Aldrich, S. *Quantum Dots - Biosensors and Bioimaging*. 2010.
20. Noblet, T., *Optical study of vibroelectronic coupling at the interface between semiconductor quantum dots and organic molecules*, in *Institute of Physical Chemistry*. 2019, University of Paris Saclay: Orsay, PhD thesis.
21. Noblet, T., et al., *A global method for handling fluorescence spectra at high concentration derived from the competition between emission and absorption of colloidal CdTe quantum dots.* Phys Chem Chem Phys, 2017. **19**(39): p. 26559-26565.
22. Thomas Noblet, S.B., Christophe Methivier, Marie Erard, Julie Hottechamps, Bertrand Busson, and Christophe Humbert, *Two-dimensional layers of colloidal CdTe quantum dots: assembly, optical properties, and vibroelectronic coupling.* The Journal of Physical Chemistry C, 2020. **124**: p. 25873-25883.
23. T. Noblet, L.D., S. Boujday, C. Methivier, B. Busson, A. Tadjeddine & C. Humbert, *Semiconductor quantum dots reveal dipolar coupling from exciton to ligand vibration.* Communications Chemistry, 2018. **1:76**.
24. Sara Mosca, C.C., Nick Stone, and Pavel Matousek, *Spatially offset Raman spectroscopy.* Nature Reviews Methods Primers, 2021. **1**(1): p. 1-16.
25. Christophe Humbert, T.N., *Unified Mathematical Formalism for First to Third Order Dielectric Response of Matter: Application to Surface-Specific Two-Colour Vibrational Optical Spectroscopy.* Symmetry, 2021. **13**(153): p. 1-26.
26. Haddada, Krafft, Vallee, A.; Methivier, C.; Boujday, S. *.et al* , *Optimizing the Immobilization of Gold Nanoparticles on Functionalized Silicon Surfaces: Amine- vs Thiol-Terminated Silane.* Gold Bull., 2013. **46**: p. 335-341.
27. Dalstein, L.H., M. B.; Barbillon, G.; Humbert, C.; Tadjeddine, A.; Boujday, S.; Busson, B. , *Revealing the Interplay between Adsorbed Molecular Layers and Gold Nanoparticles by Linear and Nonlinear Optical Properties.* J. Phys. Chem. C, 2015. **119**: p. 17146−17155.
28. Labrosse, A., *Synthesis and characterization of pure and organically modified silicas: complexing properties in aqueous medium*, in *Molecular Chemistry and Physico-Chemistry*. 1998, Université Henri Poincaré, PhD thesis
29. Kazunori Motai, T.N., Chen Chen, and Yuhei Hayamizu, *Oriented crystal growth of phenylalanine and dipeptide by solution shearing.* Journal of Material Chemistry C, 2020: p. 1-8.
30. Schrader, B., *Raman/Infrared Atlas of Organic Compounds,* . Vol. B3-02. 1989: VCH Publishers, Weinheim.
31. M.A. Bryant, J.E.P., *Surface Raman scattering of self-assembled monolayers formed from 1-alkanethiols at silver [electrodes].* J. Am. Chem. Soc., 1991. **113**: p. 3629-2637.
32. A. Ihs, B.L., *Chemisorption of -cysteine and 3-mercaptopropionic acid on gold and copper surfaces: An infrared reflection-absorption study.* Journal of Colloid and Interface Science, 1991. **144**: p. 282-292.
33. Thomas Noblet, L.D., Abderrahmane Tadjeddine, and Christophe Humbert, *Spatial Dependence of the Dipolar Interaction between Quantum Dots and Organic Molecules Probed by Two-Color Sum-Frequency Generation Spectroscopy.* MDPI Symmetry, 2021. **13**(294).